DESIGN AND REALIZATION OF A STEP MOTOR DRIVER WITH MICRO-STEPPING CAPABILITY

A THESIS SUBMITTED TO
THE GRADUATE SCHOOL OF NATURAL AND APPLIED SCIENCES
OF
MIDDLE EAST TECHNICAL UNIVERSITY

BY

EMEL HİZAL ATEŞ

IN PARTIAL FULFILLMENT OF THE REQUIREMENTS
FOR
THE DEGREE OF MASTER OF SCIENCE
IN
ELECTRICAL AND ELECTRONICS ENGINEERING

MAY 2011

Approval of the thesis:

DESIGN AND REALIZATION OF A STEP MOTOR DRIVER WITH MICRO-STEPPING CAPABILITY

submitted by **EMEL HİZAL ATEŞ** in partial fulfillment of the requirements for the degree of **Master of Science in Electrical and Electronics Engineering, Middle East Technical University** by,

Prof. Dr. Canan Özgen ______________
Dean, Graduate School of **Natural and Applied Sciences**

Prof. Dr. İsmet Erkmen ______________
Head of Department, **Electrical and Electronics Engineering**

Prof. Dr. Mirzahan Hızal ______________
Supervisor, **Electrical and Electronics Engineering Dept., METU**

Examining Committee Members

Prof. Dr. Ahmet Rumeli ______________
Electrical and Electronics Engineering Dept., METU

Prof. Dr. Mirzahan Hızal ______________
Electrical and Electronics Engineering Dept., METU

Prof. Dr. Muammer Ermiş ______________
Electrical and Electronics Engineering Dept., METU

Prof. Dr. Osman Sevaioğlu ______________
Electrical and Electronics Engineering Dept., METU

Msc. Arif Yılmaz ______________
TÜBİTAK UZAY

Date: **02.05.2011**

I hereby declare that all information in this document has been obtained and presented in accordance with academic rules and ethical conduct. I also declare that, as required by these rules and conduct, I have fully cited and referenced all material and results that are not original to this work.

Name, Last name : Emel Hizal Ateş

Signature :

ABSTRACT

DESIGN AND REALIZATION OF A STEP MOTOR DRIVER WITH MICRO-STEPPING CAPABILITY

Hizal Ateş, Emel
M.Sc., Department of Electrical and Electronics Engineering
Supervisor: Prof. Dr. Mirzahan Hızal

May 2011, 69 pages

Step motors are motion control mechanisms that convert digital pulses into mechanical shaft rotation. They provide high precision positioning and repeatability of movement without a closed loop control, which is preferable for industrial applications in which accurate positioning control is needed. In this thesis, design and realization of a step motor driver will be performed using micro-stepping, which is based on controlling the current of each winding of the motor continuously and solves noise and resonance problems as well as providing an increase in accuracy and resolution.

Keywords: micro-stepping, microcontrollers

ÖZ

MİKRO-ADIMLAMA YETENEKLİ BİR ADIMLI MOTOR SÜRÜCÜNÜN TASARIM VE GERÇEKLEŞTİRİMİ

Hizal Ateş, Emel
Yüksek Lisans, Elektrik-Elektronik Mühendisliği Bölümü
Tez Yöneticisi: Prof. Dr. Mirzahan Hızal

Mayıs 2011, 69 sayfa

Adımlı motorlar, sayısal darbe işaretlerini mekanik mil dönüşlerine çeviren hareket denetim mekanizmalarıdır. Yüksek doğruluklu konumlandırma gerektiren endüstriyel uygulamalarda tercih edilir olan duyarlıklı konumlandırma ve geribeslemeli denetimsiz hareket yinelenebilirliği sağlarlar. Bu tezde, motorun her sargısının akımını sürekli olarak denetlemeye dayalı ve gürültü sorununu çözmekle birlikte duyarlık ve çözünürlükte artış sağlayan mikro-adımlama kullanılarak bir adımlı motor sürücünün tasarımı ve gerçekleştirimi yapılacaktır.

Anahtar Kelimeler: mikro-adımlama, mikrokontrolörler

To My Beloved Husband

ACKNOWLEDGMENTS

I would like to express my gratitude and deep appreciation to my supervisor Prof. Dr. Mirzahan Hızal for his guidance and positive suggestions.

I am grateful to my family, my parents Fatma and Seyfettin and my sister Elif for their support and love.

Finally, I would like to express my special thanks to my husband, Tuğrul, for his precious help, great support and understanding. I believe without him this work would hardly be possible. This thesis is dedicated to him.

TABLE OF CONTENTS

LIST OF TABLES

TABLES

LIST OF FIGURES

FIGURES

CHAPTER 1

INTRODUCTION

A *step motor* [1,2,3,4,5,6,7,8,9,10] is a type of brushless synchronous motor that generates mechanical energy from discrete electrical pulses. Shaft of a step motor performs discrete rotation movements with respect to the input electric signal. It is possible to drive a step motor with digital signals directly from a computer or a microcontroller. In this manner, step motor drive system can be regarded as a digital to angular position converter. Along with the fact that its structure allows a simple control system, step motor has several features that make it an ideal candidate as a positioning device.

- The speed and the amount of rotation are proportional to the frequency and number of the input pulses. Thus, a wide rotational speed range can be achieved and precise positioning is possible with small angular increments.
- Accurate operation can be provided with open loop control since positional error is non-cumulative and the accuracy of a step motor is high, typically in the order of 5% of one step angle.
- Being a brushless motor, step motor is very reliable.
- Starting, stopping and reversing the device is easy.

There are also some disadvantages of using step motor. Some of which are:

- Resonances may occur at certain speed ranges.
- Step accuracy and resolution are directly dependent to the structure of the device and can be a limiting factor for applications where high resolution is needed.

Micro-stepping [11,12,13] is a step motor driving method where input pulses are converted to discrete estimations of the sinusoidal functions. This results in fractional input signals as opposed to zero, full positive or full negative input signals used in commonly employed *full-step* and *half-step* excitation methods. This method results in smoother operation with less vibration and highly enhanced angular resolution of motor control; namely, minimizes the effects of the disadvantages of step motors mentioned.

1.1 Scope

This thesis presents a step motor driver design with the aim of achieving micro-stepping capabilities. Step motors are analyzed and different driving methods including several possible control approaches are discussed. An electronic board for drive and control of a hybrid step motor with adjustable user controls has been developed and used in experiments to compare different driving strategies with respect to their electrical and mechanical performances.

1.2 Related Work

Early studies on step motors are dated back to 1920's [14]. Although the same motor structure was known and used as an electromagnetic engine in the 19^{th} century, a three-phase variable reluctance step motor was introduced as a position control device in an article named "*The Application of Electricity in Warships*" for the first time [4,14]. In this article, a 3-phase variable reluctance step motor and a mechanical rotary switch that causes motor to move in steps of 15° were described [4]. Inventions which enhanced step accuracy and torque capability of step motors proceeded gradually [15,16] and the use of permanent magnets in step motor structure was introduced in this period. *Hybrid step motor*, which is widely used today, was invented, patented [17] and manufactured by General Electric Company in 1952. First examples of this motor were used as synchronous motors running at low speeds. However, hybrid motors have been used increasingly as a position control device ever since. Especially, in 1960's and 1970's, evolving computer technology has also led an improvement in step motor technology. Computer manufacturers, such as IBM, has used step motors as actuators in terminal devices and promoted production of high performance step motors.

In addition, as microprocessors become widespread, the use of step motors became easier and more preferable due to the discrete nature.

Since the roots of step motor applications are found nearly a century earlier from now, it is possible to observe almost all footsteps of the digital control history by reviewing step motor drivers used throughout time. As mentioned before, first examples utilized to excite step motors were manual mechanical switches. Later, with the invention of switching devices such as thyratron gas tubes, more complicated and autonomous driver options have become in use. A widespread implementation was an information storage application. Operation instructions for numerically controlled machines were stored in the form of perforations on tapes and a sensing device was used to convert the information on the tape to the control signals for the switches. These switches were gradually replaced by thyristors and transistors. With the appearance of the integrated circuits, the implementation of logic circuit of drivers became simpler with lower costs.

Step motors are attractive and widely used in the industry due to their low price, simplicity and low cost driver solutions. There are various alternatives to implement the power converter block of a driver, partly or whole *on-chip* solutions are provided by various manufacturers. L297-L298 IC's from ST Microelectronics is among the classic and popular driver solutions. In 2006, ST announced a new 65W fully integrated step motor driver IC [18]. Ji *et al.* [19] proposes an application circuit utilizing DMOS full-bridge motor driver IC LMD18245 [20] from National Semiconductor.

There are also highly sophisticated single chip solutions for driving step motors in the market today. Allegro's A3981 [21] and A4980 [22] and AMIS-30523 [23,24] from ON Semiconductor (formerly AMI Semiconductor) are some examples of this type of drivers. Although on chip solutions offer simple construction, a fully-functional drive circuitry with a few external components; discrete driver solutions are still widely used. One reason for this is that the maximum output power capability of the system is limited in on-chip solutions. Power converter block constructed with discrete components gives more flexibility in this case. Similarly, drive control logic circuitry options are also limited and cannot be changed for most integrated driver IC's. However, a *PCB* level driver with driver logic being handled by a microcontroller device offers a flexible environment to improve various driver algorithms.

The core component of a PCB level step motor driver is the processor where driver logic is generated. Besides microcontrollers, *DSP*'s (Digital Signal Processor) are also widely used as processors in step motor drivers. An application report from Texas Instruments describes an implementation of a micro-stepping algorithm for TMS320F2808 DSPs [25]. Bellini *et* *al.* [26] presents a micro-stepping implementation where a DSP is utilized as the processor of the driver where a new *pulse width modulation* (PWM) method, which is called as *mixed-mode PWM*, is proposed.

Field Programmable Gate Array (FPGA) based step motor driver solutions were also implemented in recent years [27,13,28], although not as very widespread as microcontrollers or DSP's. Le and Jeon [27] propose an open-loop step motor driver based on FPGA. Although FPGA based solutions are relatively a harder to implement and more costly, their rationale is that FPGA based designs are compatible with *Application Specific Integrated Circuit* (ASIC) conversion and thus they may be preferred. Another example to FPGA based solutions is the work of A. Astarloa *et al.* [13] where they propose a step motor control system which achieves the control of the micro-stepping resolution on-the-fly; which most of the step motor driver systems cannot offer, by dynamically reconfiguring block RAM in the FPGA used as the processor of the driver.

An application note from Microchip [29], introduces a step motor driver implementation realized with a new generation *PIC* family, called the *dsPIC*. The study covers different controlling schemes and micro-stepping options with several resolutions. Part of this thesis is built upon the ideas presented in this application note.

Ran Zhang *et al.* [30] present a PIC18F2331 [31] based step motor driver with closed-loop current control using micro-stepping method for a two-phase hybrid step motor. In this study, a high and low side driver IR2110 [32] is used to drive the discrete power block elements and cycle-by-cycle current limiting, a feature of the driver IC, is utilized to control current output of the driver. The study presented in this paper matches with the design presented in this thesis work on the grounds that parallel approaches are used and also PIC18F4431 [31], a PIC in the same family with PIC18F2331, forms the core of the realization of the driver presented in this thesis work.

Many other studies on step motor driving exist in the literature. Different driving approaches exist for different step motor structures, such as linear motors [12]. A driving scheme for 5-phase step motors is proposed in [33]. Step motor modeling is a major area where Morar [34] discusses accurate simulation modeling of step motors. Closed-loop positioning methods form another major area [35]. Brown et al. [7] introduce a damping circuit to solve oscillation problems.

1.3 Outline

This thesis contains six chapters. Chapter 2 introduces step motors which are the mechanical components to be driven with the driver circuitry and Chapter 3 provides a discussion on step motor control methods. The proposed driver circuit is presented in Chapter 4. Chapter 5 discusses experimental work and their results. Finally, Chapter 6 puts forward conclusive remarks and future directions.

CHAPTER 2

STEP MOTOR THEORY

S*tep motors* are brushless synchronous motors which perform a full rotation cycle in a fixed number of steps. Theory of step motors deals with operability, physical structure and their driving approaches along with electromechanical analysis of their operation.

This chapter deals with the fundamental ideas behind step motor theory. The discussion is opened with the basic operation principle of step motors in the first section. The second section introduces different types of step motors in use and different winding structures are mentioned in the third section. Afterwards, several methods that are used to excite and operate step motors are discussed. *Micro-stepping* method, a primary focus of this thesis, is presented in this fourth and final section.

2.1 Basic Operation of Step Motors

Mechanical operation of step motors is possible with moving active parts with magnetic force which is induced with discrete electrical signals. A basic type of step motor, called the *variable reluctance step motor*, consists of stator and rotor parts made of ferromagnetic material, such as steel. This section explains the principles of motion inside a simple 3-phase variable reluctance motor in order to make an introduction to the basic concepts of step motors. Different types of step motors and excitation modes are discussed in following sections in more detail.

Basic structure of a variable reluctance step motor is shown in Figure 1. This motor has a stator with six teeth and a rotor with four teeth and both parts are made of steel with high permeability allowing high magnetic flux flowing through the structure. The stator is wound in a 3-phase arrangement as shown in Figure 1 (b). Each phase (A, B or C) connects two opposing stator teeth in series and induces a directed magnetic flux along the diameter when excited.

In a simplified configuration, each phase of the stator is connected to the DC power source through a switch. Phases of the stator are energized; in technical terms *excited*; in a sequence by means of controlling the switches. Basic operation of the motor relies on the principle that rotor aligns itself with the position where the magnetic reluctance is at minimum and the magnetic flux produced is at maximum. This position is called *equilibrium position* or *rest position*.

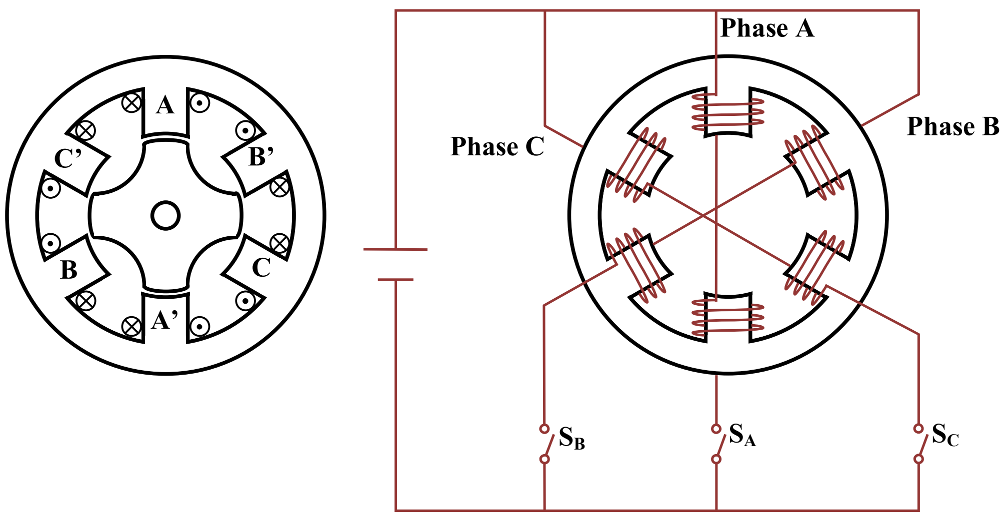

(a) (b)

Figure 1 Cross sectional diagram of a 3-phase variable reluctance step motor. (a) Stator and rotor teeth. (b) Winding arrangement.

Figure 2 (a) shows the rest position of the rotor when only phase-A winding is excited. The rotor is magnetized and aligned with the flux lines. If excitation switches from phase-A to phase-B, magnetization of the rotor changes with new flux lines. In order to reduce the air gap in which the magnetic flux occurs and reduce the *Maxwell stress* [36], the rotor starts moving in counter-clockwise direction towards a position with lower reluctance as shown in Figure 2 (b) and finally reaches the rest position as shown in Figure 2 (c).

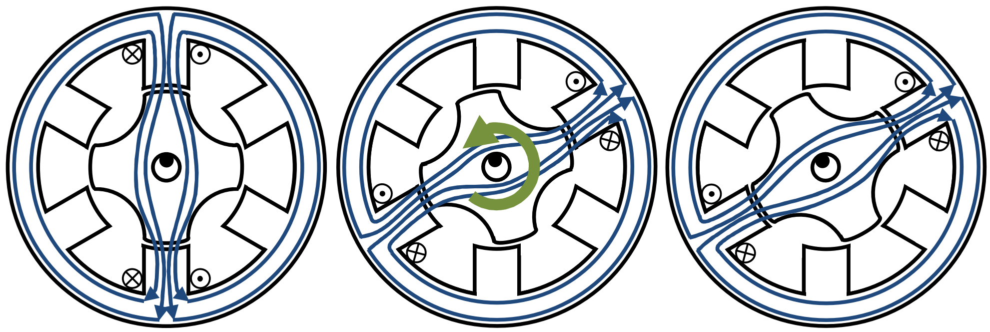

(a) (b) (c)

Figure 2 Rotor position at (a) excitation of phase-A, (b) some time after excitation of phase-B and (c) stable position after excitation of phase-B.

The amount of rotation of the step motor between two consecutive equilibrium positions in two different phases is called the *step angle*. Step angle is related to the number of stator phases (p) and rotor teeth (N_r) and its value is governed by (1). Thus the variable reluctance motor having three phases and four rotor teeth, as depicted in Figure 1, has a step angle of 360º/(3·4) = 30º. The number of steps required for a full rotation of rotor back to its initial position, or the *step number*, is 12 in this case.

$$\theta_s = \frac{360°}{p \cdot N_r} \tag{1}$$

The flux lines flow downwards when the stator windings of phase-A is excited and phase-B and phase-C are switched off. This causes the stator tooth at A magnetized to north pole and the stator tooth at A’ magnetized to south pole. Similarly the rotor tooth pointing upwards in cross-sectional representation is magnetized to south pole and the rotor tooth pointing downwards is magnetized to north pole.

Consider the case where phase-A windings are arranged in a reverse manner so that the induced magnetic flux flows upwards. In this case, pole configurations would reverse but the rest position will not change. Thus, rotation direction or step size does not depend on the direction of flux for this type of motor.

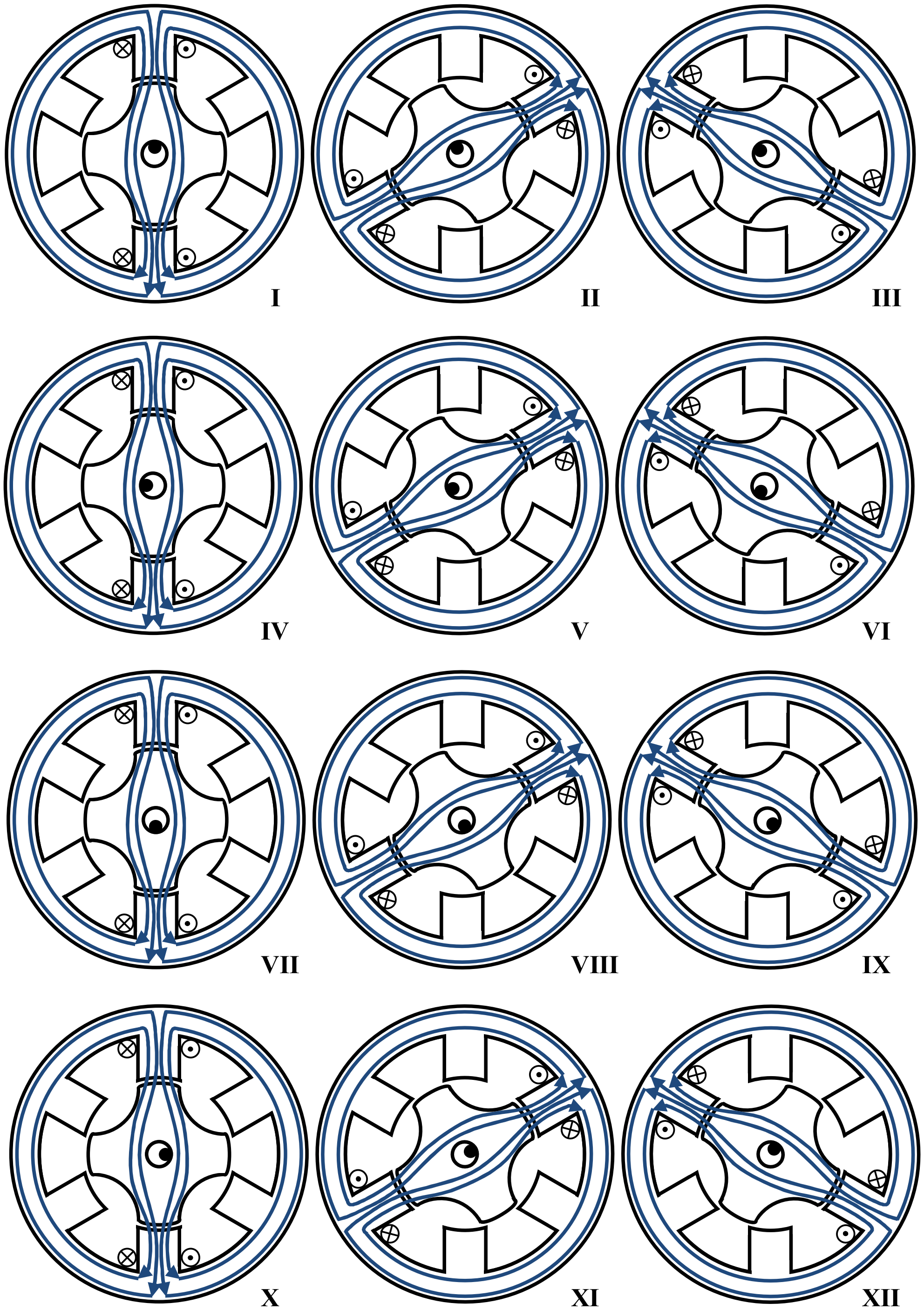

Figure 3 Full revolution of a step motor with a step angle of 30°.

A switch from phase-A to phase-B causes the rotor to rotate 30º counter-clockwise. Similarly, a switch from phase-B to phase-C will cause the rotor to rotate 30º more degrees to the same direction. A full revolution is completed in twelve steps as shown in Figure 3 where phase windings are excited in successive repetition. A small dot placed on the rotor shaft indicates a reference mechanical angle.

A rotation in clockwise direction can be achieved by reversing the excitation order. Successively switching from phase-A to phase-C, afterwards to phase-B and finally back to phase-A will cause the rotor to rotate in the reverse direction with the same step size.

2.2 Types of Step Motors

The core idea in the operation principle of step motors is the fact that the rest position of the rotor changes by a fixed angle amount when excitation switches from one phase to another. This process is elaborated in the previous section with a variable reluctance motor which consisted of ferromagnetic mechanical components only.

This section lists and describes different types of step motors according to their magnetic structure and how magnetic flux triggers the motion of their rotors. Firstly, the *variable reluctance motors* are discussed further and several different variants are given. The second type of step motor is the *permanent magnet motor,* which utilizes permanent magnets to perform electromechanical rotation. Finally, the *hybrid step motors* combine mechanical and electromagnetic properties of the former two types to achieve higher torque within the same physical volume.

2.2.1 Variable Reluctance Step Motors

Variable reluctance step motors consist of wired iron rotors and wound stators. In a variable reluctance motor, stator poles are excited with DC input and rotor windings become attracted and perform rotation. A 3-phase variable reluctance motor with six stator teeth and four rotor teeth is presented in Figure 1.

A change in DC input from one phase to another changes the amount of actual air gap and thus the amount of instantaneous reluctance present under magnetic flux lines. The step motor reaches an equilibrium position when the rotor teeth under magnetic flux align with the excited phase.

Step motors in use generally have step angles much lower than 30º. A lower step angle is achieved by increasing the number of phases and rotor teeth. Figure 4 (a) shows a variable reluctance step motor with eight stator teeth and six rotor teeth. A single step in this motor results in 15º of rotation. This motor sacrifices ease of control with an additional electrical phase in order to obtain a higher step number.

An alternative approach to increase the step number is using two or more teeth per pole. A 3-phase variable reluctance motor structure with 14 rotor teeth is given in Figure 4 (b). This motor attains a step number of 42 and a step angle of 8.57º.

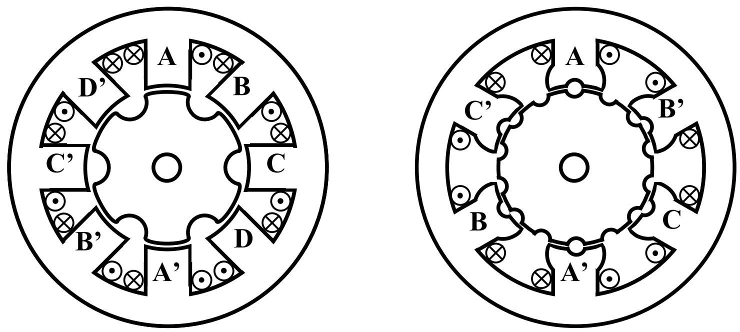

(a) (b)

Figure 4 Cross sectional view of (a) a 4-phase variable reluctance step motor and (b) a 3-phase variable reluctance step motor with two teeth on each pole.

2.2.2 Permanent Magnet Step Motors

Permanent magnet step motors have cylindrical magnet rotors and single pole electrical phases. When a phase is excited, magnetic flux occurs inducing north or south pole on a single stator teeth, which in turn aligns the permanent magnet rotor inside. Illustration of a permanent magnet step motor is shown in Figure 5.

The rotor of a permanent magnet motor stays at a *detent position* enforced by the magnetic structure of the motor when no excitation is in place. This position can be different from the rest position of the motor when any of the windings are excited.

Similar to a variable reluctance motor, rotation in a permanent magnet step motor is realized by alternating excitation between consecutive phases. The rotor inside the motor given in Figure 5 rotates clockwise when phase excitation order is A-B-C-D. Exciting the stator winding in A-D-C-B order will result in a counter-clockwise motion. Step angle of this motor is 90º. Step angle of permanent magnet motors can be decreased by introducing more stator teeth and phases.

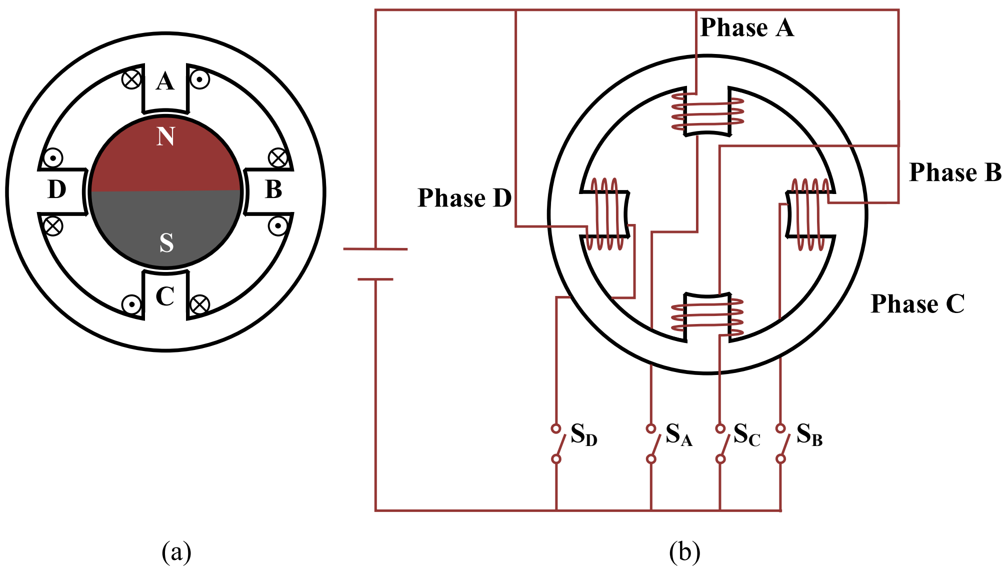

Figure 5 Cross sectional diagram of a 4-phase permanent magnet step motor. (a) Stator teeth and cylindrical magnet rotor and (b) winding arrangement.

The permanent magnet step motor, whose windings are shown in Figure 5, is excited with *unipolar* winding excitation where current flows towards a single direction. In this example, each stator teeth is excited to south pole with the windings coiled around. This configuration results in an inefficient operation in terms of generated torque since opposing stator teeth with respect to stator magnetization are not utilized. The alternative is the *bipolar* winding excitation where stator windings can be excited in both directions. In this configuration opposing stator teeth are excited to opposing poles, i.e. Pole C is magnetized to north when pole A is magnetized to south, and the induced magnetic flux increases as well as the generated torque per motor volume. In bipolar excitation, opposing poles are regarded as a single phase and they are named such as A, B, A’ and B’ instead of A, B, C and D. Detailed discussions on different winding configurations are given in the next section.

2.2.3 Hybrid Step Motors

Hybrid step motors combine operation principles of both variable reluctance motors and permanent magnet motors. In a typical hybrid step motor, the rotor structure is cylindrically *stacked* into two more sections as shown in Figure 6 (a). Interior of the rotor is a cylindrical permanent magnet with different poles in consecutive stacks and the teeth of the rotor are laminated steel. Different stacks have a fractional tooth pitch difference.

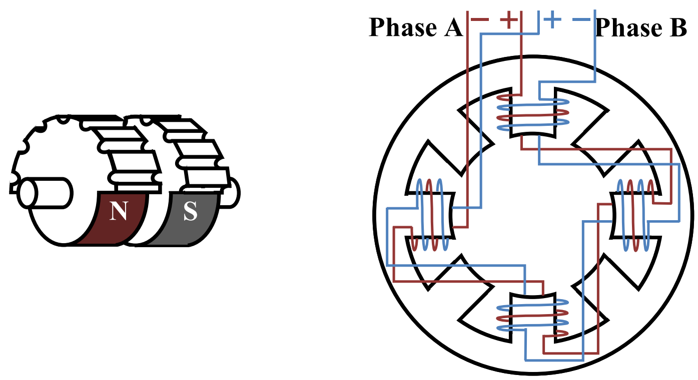

(a) (b)

Figure 6 (a) Teeth and magnetic structure of the rotor of a hybrid step motor. (b) Bifilar windings of two phases of a 4-phase stator of a hybrid motor.

The stator structure of hybrid motors with misaligned rotor teeth are not different from stator structures of other motor types covered so far. However, the windings are arranged in *bifilar* scheme that allows induction of magnetic flux in both directions. Bifilar filing in a two phase hybrid motor is shown in Figure 6 (b). In a hybrid step motor, during excitation of phase A, both magnetic poles of the rotor become attracted and align to a specific position. When excitation switches to phase-B, the rotor teeth become attracted in the opposing direction and movement is realized in a specific direction designed by proper teeth alignment.

Different variations of hybrid motors can be obtained either by using a permanent magnet as the stator instead of the rotor or by enforcing teeth misalignment to stator stacks instead of the rotor.

2.3 Step Motor Winding Types

2.3.1 Monofilar and Bifilar Winding

Each winding spans two opposing stator teeth in a variable reluctance motor which is shown in Figure 1 and each winding spans a single stator teeth in a permanent magnet motor which is shown in Figure 5. Each coil around a single stator tooth belongs to a single phase in both motor types. This is called the *monofilar winding* scheme. Figure 1 (b) and Figure 5 (b) shows examples of this winding type.

Windings in a hybrid step motor share stator poles, in contrast to monofilar winding. Thus, both magnetic poles can be realized on a single stator tooth. This is called the *bifilar winding* scheme and an example is seen in Figure 6 (b).

Two coils wound around a single tooth are magnetically coupled when an excitation on any of them is applied. This coupling allows better positioning than wiring these two coils separately[4].

2.3.2 Unipolar and Bipolar Winding Drive

Same voltage polarity applied to monofilar windings will create a magnetic flux always in the same direction. The stator tooth around which the coil is wound will have a single magnetic polarity dictated by the winding orientation. This kind of excitation is called the *unipolar drive* of the winding. A simple circuit for unipolar drive on a monofilar winding is shown in Figure 7 (a). A transistor in series allows switching the excitation current on and off.

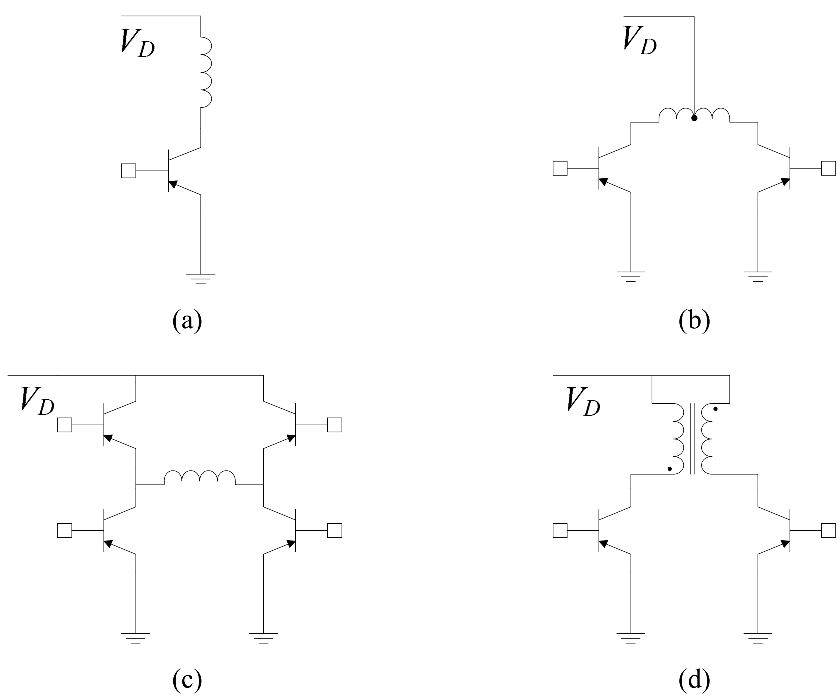

Figure 7 (a) Monofilar winding, unipolar drive, (b) Unipolar drive with a center-tap (c) monofilar winding, bipolar drive and (d) bifilar winding, bipolar drive.

Permanent magnet and hybrid step motors require attraction of both magnetic poles. *Center taps* are used to achieve this with unipolar driven windings as shown in Figure 7 (b). A 2-phase permanent magnet or hybrid step motor with a unipolar winding structure has five or six wires, composed of two terminals for each winding and one combined or two center taps respectively. These center taps are typically used as the positive supply side, and the terminals of the windings are grounded. In this step motor winding configuration, two switches are required, one for each half of the winding. Only a single half of the winding can be excited at a time and the torque output reduces as a result.

Current on a monofilar winding can induce a magnetic flux in the opposing direction if it is flowing through the coil in reverse. Selectively changing the flux direction, thus magnetic polarity, can be achieved with the *full-bridge* converter given in Figure 7 (c) with four transistors. This excitation technique is called the *bipolar drive* of the monofilar winding. The full-bridge topology is discussed in Chapter 4.

The winding structure of bipolar step motor does not have center taps. A 2-phase permanent magnet or hybrid step motor with a bipolar winding structure has four wires as shown in Figure 7 (c). In this configuration, the whole winding can be energized at once as opposed to the unipolar drive with a center tap. As a result, the torque capability of the motor can be fully utilized. However, the bipolar drive circuitry is more complex than the unipolar driving circuitry.

Finally, the bifilar winding method allows inducing magnetic flux in any direction by selectively exciting one of the coupled coils. Bipolar drive of the bifilar scheme is shown in Figure 7 (d).

2.4 Step Motor Excitation Modes

In the examples given so far, only one phase of any step motor is excited at any time during rotation. In this section different phase excitation approaches are presented. First of all, the basic method of *wave drive excitation* is given and it is followed by *two-phase on excitation*, which is an alternative to produce full steps. The discussion continues with *half step excitation*, which doubles the effective step number and thus increases the positional accuracy. Finally, *micro-stepping excitation*, which is the most important of all regarding this thesis, is explained.

2.4.1 Wave Drive Excitation

Wave drive excitation is the step motor excitation method where only a single phase winding is excited at a time. All phases are excited one by one in an alternating sequence as represented in Figure 8. In wave drive excitation, each clock rotates the rotor by one natural step angle, θ_s. This makes wave drive a method for *full-step excitation* of the motor, since it causes rotation in full steps. The sequence given in Figure 8 rotates a 3-phase variable reluctance motor as shown in Figure 3.

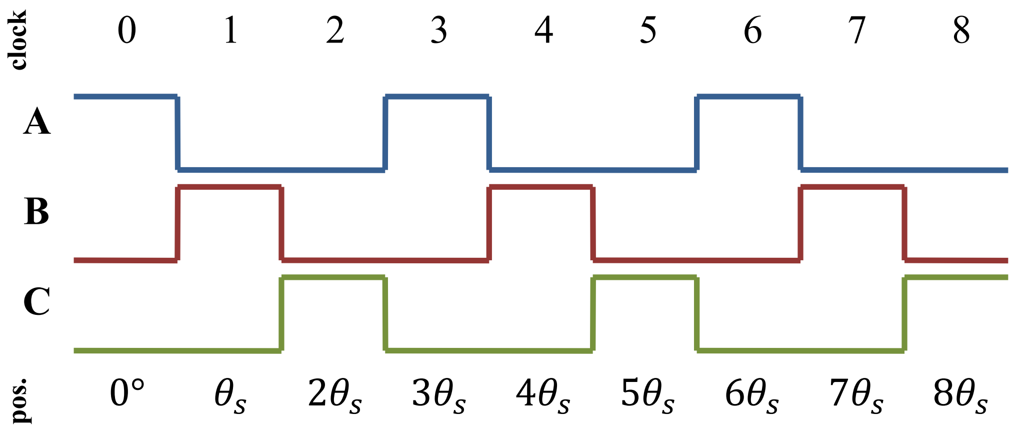

Figure 8 Wave drive excitation sequence for a 3-phase step motor.

2.4.2 Two-Phase On Excitation

Two-phase on excitation is the step motor excitation method where two phase windings are excited simultaneously at a time, as the name implies. This operation is also called *full-step excitation* since it causes rotation in full natural steps. Similar to the wave drive, two-phase on excitation is a full step operation. The polarity of the input is reversed for one of the phases each time to trigger a new step. This results in full rated torque. The excitation sequence for a 3-phase motor is given in Figure 9.

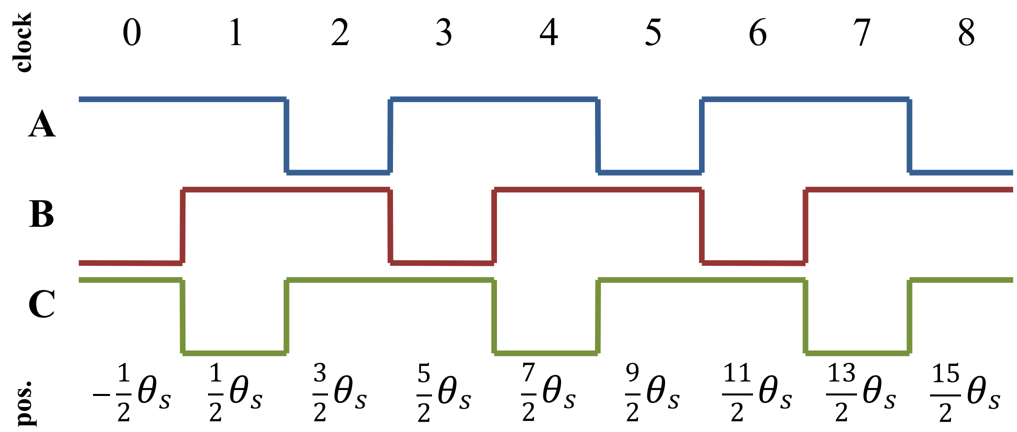

Figure 9 Full-step excitation sequence for a 3-phase step motor.

Excitation of two phases together provides a better transient response than exciting a single phase only. The details of this phenomenon can be found in the fourth chapter of [4] where further information on the dynamical analysis of one-phase on and two-phase on excitation modes and comparison of their damping characteristics is given. Figure 10 shows the step transition in two-phase on excitation from phases A and C to phases A and B of the variable reluctance motor given in Figure 1.

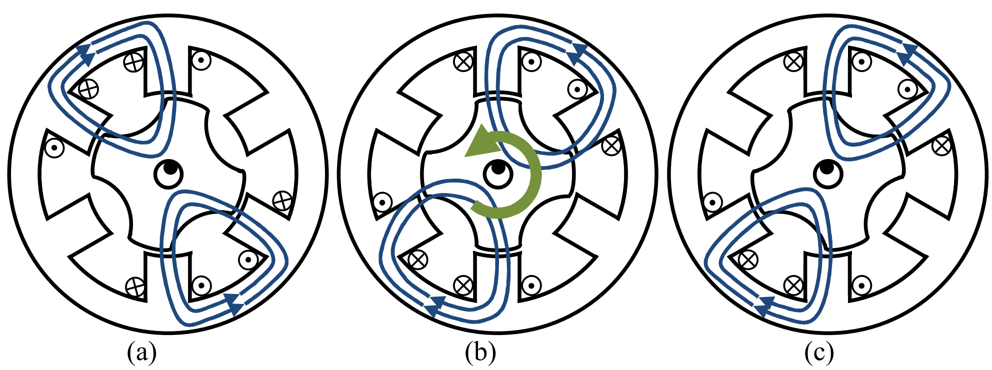

Figure 10 Rotor position at (a) excitation of phase-A and phase-C, (b) some time after turning off phase-C and turning on phase-B and (c) stable position after excitation of phase-A and phase-B.

2.4.3 *Half-Step Excitation*

In *half-step excitation*, a step motor driver switches between two-phase on excitation and wave drive excitation. The combined sequence for a three phase motor is shown in Figure

11. All possible rotor positions from both wave drive excitation and two-phase on excitation are available in half-step excitation, reducing the effective step angle to half. This operation results in higher angular precision but lower torque.

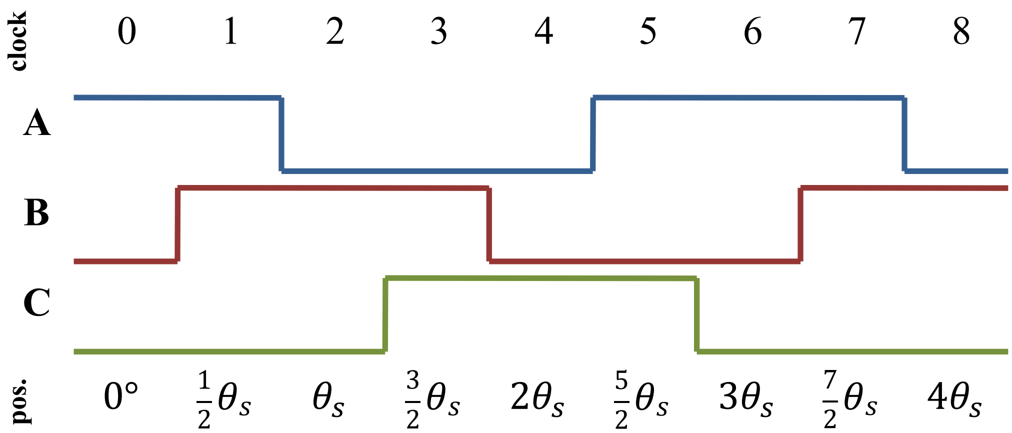

Figure 11 Half-step excitation sequence for a 3-phase step motor.

2.4.4 Micro-Stepping

This thesis focuses on *micro-stepping* excitation method, which is based on subdividing one natural step of a step motor into many small steps with use of electronics [3,4].

In traditional drives, stator phases are excited with discrete pulses [26]. This type of excitation brings some limitations to the motor operation. One limitation is, step size, therefore system position accuracy is generally bounded to the natural step size of the motor, which is directly determined by the stator phases and rotor teeth count. Another limitation is the poor dynamic torque characteristics. One way to overcome this problem is to generate new intermediate equilibrium positions [26] to smoothen the motor operation. An example to micro-step excitation sequence for a 3-phase step motor is shown in Figure 12.

In wave-drive and two-phase on excitation, step size is equal to the natural step size. In half-step excitation, step number is doubled and step size is halved. This is achieved by mixing equilibrium positions from the wave-drive and two-phase on methods. On the other hand, micro-stepping method divides one full-step into a large number of smaller discrete steps by continuously varying winding currents [37].

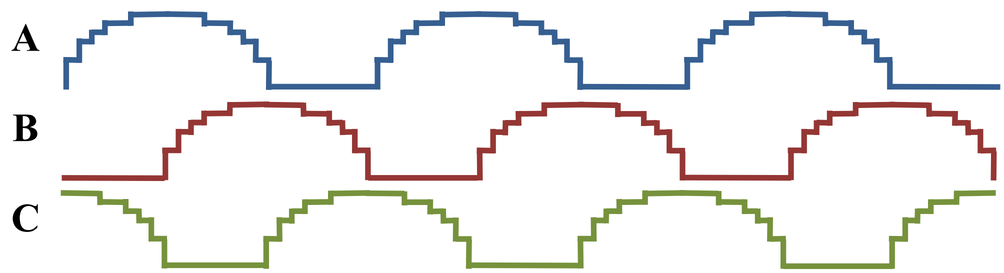

Figure 12 Micro-step excitation sequence for a 3-phase step motor.

Assuming an ideal micro-stepping drive system by neglecting the non-linear effects of both the motor and the driving circuitry, currents of a two-phase hybrid step motor can be represented as a space vector [38,26] given in (2). Amplitude of the resultant current vector $\boldsymbol{i}$ remains constant and is equal to I if phase currents are chosen as in (3) and (4) where θ_e is the electrical position and I is the current amplitude per phase.

$$\boldsymbol{i} = i_a + j\, i_b \tag{2}$$

$$i_a = I \sin \theta_e \tag{3}$$

$$i_b = I \cos \theta_e \tag{4}$$

As shown in Figure 13, produced torque of the motor will be constant over the full operation cycle since torque is directly proportional to current. In other words, the torque behavior under sinusoidal excitation and the full step equilibrium position will be the same. Thus, it is at least theoretically possible to obtain infinitely many intermediate equilibrium positions [38,26]. However in practice, non-linear factors of the system bring restrictions on the number of *micro-steps* achievable and also introduce difficulties in achieving constant current and torque outputs. Yet, micro-stepping method can significantly improve system performance.

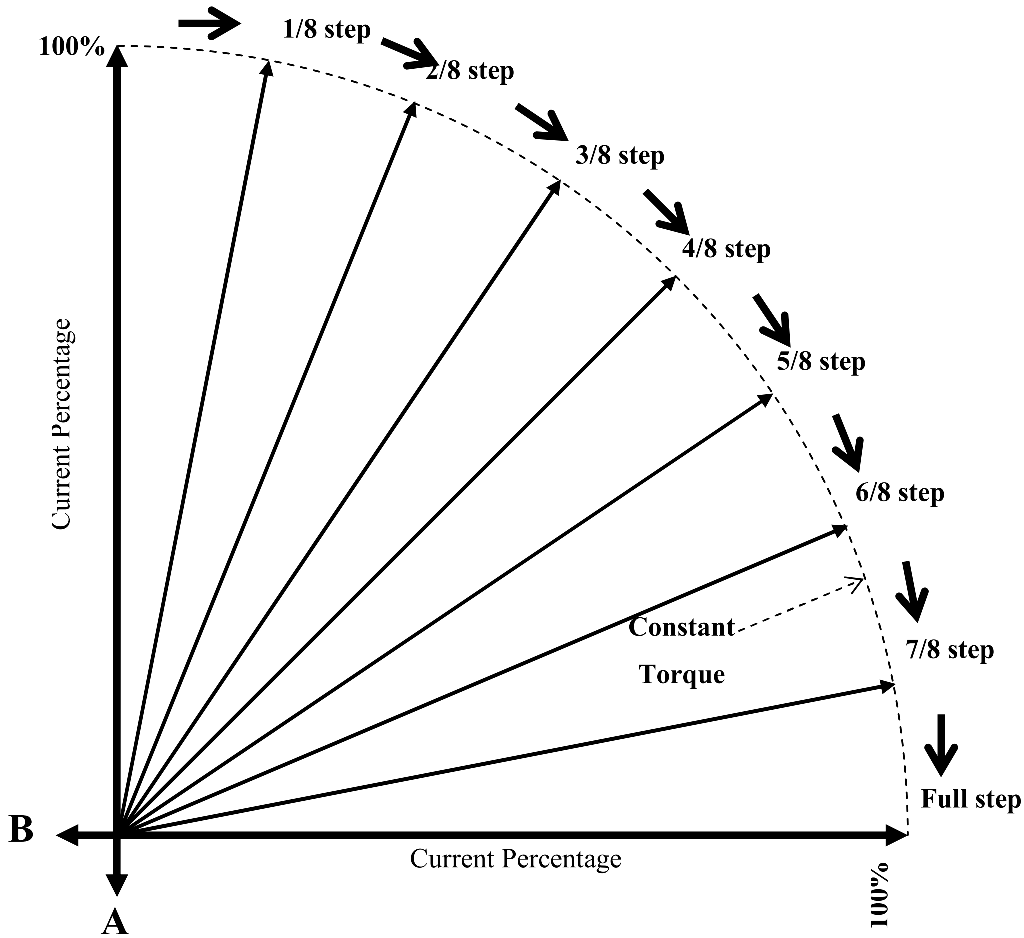

Figure 13 Space vector representations of phase currents in a 1/8th micro-stepping operation.

CHAPTER 3

STEP MOTOR CONTROL METHODS

A step motor control system is composed of three parts as shown in Figure 14. Apart from the motor itself, which performs the actual electromechanical conversion, a step motor control system includes a motor *driver* which is a piece of electrical circuitry that provides the required electrical signals to rotate or hold the step motor according to its control inputs. These control inputs are generated by a *controller* of the step motor control system. A step motor controller is the unit that produces input pulses for motor drivers to control an outer mechanical structure with step motors. A velocity profile is used to bring step motors into specified positions at specified time intervals.

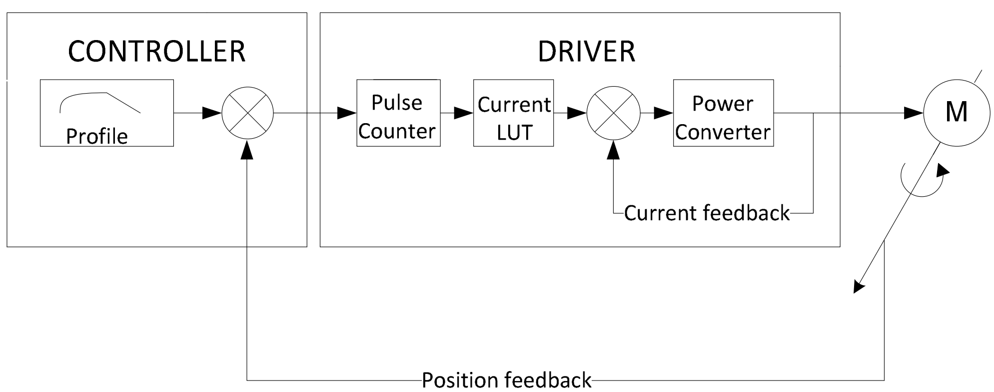

Figure 14 A generalized step motor system with a position and current feedback path.

Input pulses brought to a step motor driver are used to control the number of *steps* or *micro-steps* to apply to the motor. Generally, these input pulses are converted into iterations using a *look-up-table*, which stores the amount of current to supply to each phase of the motor in a micro-stepping application.

The first section of this chapter deals with the methods used in controlling the position of the step motor whereas the second section deals with the types of current control methods of the motor driver. These methods are associated with the position and current feedback loops, which are shown in Figure 14.

3.1 Position Control Methods

Step motors perform rotation by switching between equilibrium positions. Rotor position is known to the driver at any time if the initial position is known and the motor is operating properly under no load. Thus, it is possible to drive a step motor by directly sending appropriate electrical signals to bring the rotor into a specific position without using a position feedback loop. This technique is called the *open loop position control* of the step motor.

A load which is connected to the shaft of the step motor can manipulate the rotor position if it applies an amount of torque that is higher than the *equilibrium torque*, which is caused by the magnetization from stator windings at an equilibrium position. If the load range is small enough, open loop control can still be utilized by increasing the equilibrium torque to compensate for the load. On the other hand, accurate positioning under a wide range of loads can be achieved by *closed loop position control* of the step motor where rotor position is converted to electrical signals by a sensing mechanism and returned to the controller with a feedback path. The controller can respond to the load by adjusting the speed until the rotor comes to a desired position.

In a closed loop position control system, instantaneous rotor position is measured and fed back to the system during operation. Thus, the synchronism is ensured continuously between step commands of the controller and rotor position. The system processes the next command after the controller receives the information that the former step is completed and hence the rotational acceleration of the rotor is adjusted automatically.

Acarnley [39] proposes two methods for position detection mechanism which are *optical detection* of rotor position and *waveform detection*. Optical position detection is based on utilizing an optical encoder, which is a directly connected to the rotor shaft, measures the angular displacement of the shaft and converts this information to a proper electrical signal. Drawbacks of this method are the additional cost of encoder and additional mechanical connections introduced to the system. Waveform detection overcomes both of these drawbacks by monitoring the phase currents of each phase of the motor and analyzing their waveforms [39].

Closed loop systems are superior to the open loop systems when utilization of the torque capacity of the system is considered since it is necessary to use a closed loop system in order to run the system in full torque capacity without stalling the motor. On the other hand, the reason why step motors are popular in the market is their ability to operate without a position control mechanism. For applications with light load requirements open loop position control generally suffice.

3.2 Current Control Methods

The aim of current control is managing the power which is supplied to the step motor. Similar to position control, current can be controlled in either an open loop or closed loop fashion.

Open loop current control refers to the control of the step motor without measuring the current flowing through the windings. One of the simplest of open loop control methods is the *fixed voltage control*, which is preferred for systems where torque demand of the system is not critical. Fixed voltage control method aims to provide a fixed amount of voltage, which is generally the rated voltage, to drive the motor and current limitation is left to the internal resistance of the motor [40]. Fixed voltage control is ideal if low noise operation is needed and the system is operated under fixed conditions such as fixed motor speed or fixed load [29].

In systems with a higher torque demand, *fixed current control* is employed where the motor is operated around the rated current. Fixed current control method refers to open loop current control as in the case in the fixed voltage control. This time, the voltage level applied to the windings is increased. As a result, output current of the driver can reach to the desired levels more rapidly and thus allows faster operation.

Current control can be implemented in various ways. One approach is directly applying the rated voltage to the phase windings in a sequence in accordance with the desired excitation mode. This is the method mentioned as fixed voltage control. Another option is using a power source with a higher voltage than the rated voltage of the motor. Stepping this voltage down to the rated voltage is achieved either by applying linear control or by a *pulse width modulation (PWM) chopper* [29,40] as shown in Figure 15.

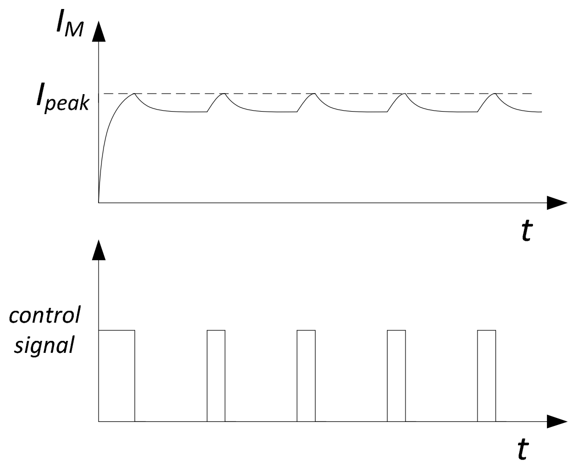

Figure 15 Control of motor current with a PWM chopper.

The classical scheme of current limiting techniques, which is referred as *L/R drive,* was commonly used and recommended until 1980's to overcome the slew rate problem of voltage control [40]. Slew rate problem is the inability of output current to instantaneously settle after excitation due to the inductive nature of the motor.

The step motor can be modeled as a series L/R circuit. At the time of excitation, (5) and (6) are valid where L_m and R_m are motor parameters and τ is the time constant of the circuit.

$$V_{bus} = L_m \cdot \frac{di}{dt} + R_m \cdot i \tag{5}$$

$$\tau = \frac{L_m}{R_m} \tag{6}$$

The more dominant the inductive behavior, the lower the slew rate of the output is. Time constant of the drive is increased by adding a series resistor, as in (7) and (8).

$$V_{bus} = L_m \cdot \frac{di}{dt} + (R_m + R_{ext}) \cdot i \tag{7}$$

$$\tau = \frac{L_m}{(R_m + R_{ext})} \tag{8}$$

It is possible to have a higher bus voltage than in the former case. $V'_{bus} > V_{bus}$ is applied to the windings. The new circuit with added R_{ext} and the output current are given in Figure 16 (a) and (b) respectively.

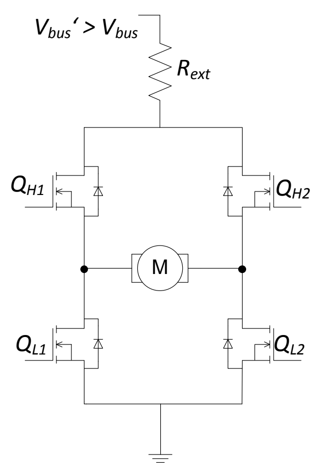

(a)

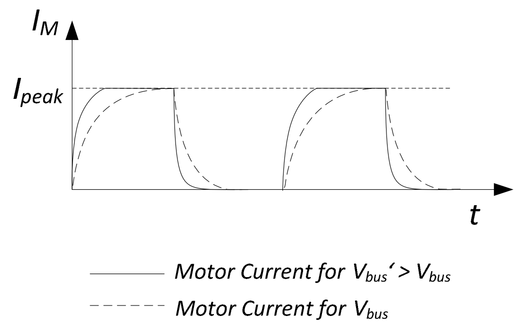

s

(b)

Figure 16 (a) L/R drive circuit and (b) switching response of its output current.

Step motor systems that incur a varying amount of torque from their load can utilize *closed loop current control*, where output current is measured and adjusted according to torque demands. Closed loop current control offers a better performance compared to open loop current control.

Closed loop current control can be achieved with peak detection [41] where the peak value of the phase current over many steps is detected and regulated by adjusting the duty cycles of the PWM signals accordingly. Achieving this type of regulation is possible with a PWM chopper on a full-bridge topology [29]. A low starting reference value is selected and the duty cycle of the PWM signal is gradually increased until the maximum measured current value is equal to the rated current of the motor. The measured maximum current is sampled for each electrical cycle and the fixed current control is implemented continuously. As a result, motor performance under variable speed conditions significantly increases. This method also has the advantage of operability with different step motor types. Prior tuning specific to the motor type is not required [29].

It is also possible to adjust the whole shape of the current waveform with closed loop current control where system measures the winding currents forces them to follow a reference pattern.

PI control is a generic framework for process output manipulation and can be utilized for matching step motor current to specific waveforms [29]. In a PI step motor controller system, the difference, or *error*, between measured and desired instantaneous current, also called the *set-point*, is collected and summed with its integral to generate a PI output as shown in Figure 17. A negative PI output invokes an inhabitation of output current and a positive output leads to a boost.

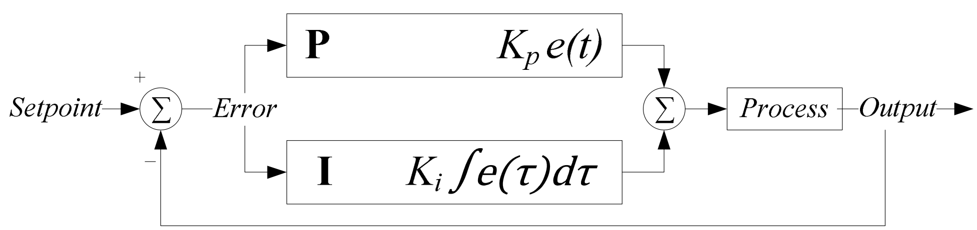

Figure 17 Block diagram of PI control.

A step motor driver utilizing a closed loop PI current controller can gradually adjust its operation according to the PI block output, e.g. by altering the duty cycle of its PWM generator [27]. Shutting off current supplies to the motor on negative PI output is another option [30].

CHAPTER 4

PROPOSED SYSTEM

Step motors are devices that convert discrete electrical pulses into mechanical rotation. A *hybrid step motor*, which combines the principles of both variable reluctance and permanent magnet motors, is an efficient and widely utilized step motor type.

A step motor control system is composed of controller and driver parts. Motor controllers are devices that drive a step motor according to a predefined velocity profile. On the other hand, a step motor driver is responsible for the generation and timing of electrical pulses to perform rotation as well as the driving of the current to energize the motor windings.

This chapter introduces the step motor driver circuit, which is designed and implemented as part of this thesis. This driver performs the bipolar micro-step excitation of 2-phase hybrid step motors.

Generation and timing of electrical pulses to generate motor steps are accomplished in a functional unit which is called the *digital control* of the driver. These pulses are passed to *gate drivers*, which shift the level of electrical inputs to operate a set of switches inside the *full-bridge converters* introduced in Chapter 2. The full-bridge circuit drives the current for the motor windings according to electrical pulse inputs.

The overall view of the whole driver system is introduced in the first section to provide a general discussion on the problem. The chapter continues with the full-bridge converter in the second section, with the gate driver in the third section and with the digital control counterpart in the fourth section. The fifth section deals with the closed-loop current control in this driver.

4.1 *Overall System*

Step motor driver system implemented in this thesis is divided into three components. *Digital control* generates the logical signals that form a micro-stepping waveform. These signals are converted electrical levels for transistor gate switches by *gate drivers*. Finally, a *full-bridge converter* is used to drive each phase of the step motor. Overall architecture is summarized in Figure 18.

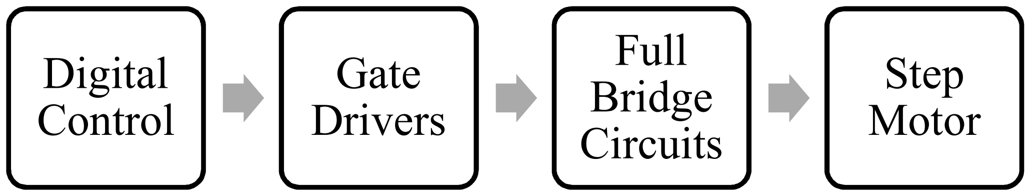

Figure 18 Overall motor driver system.

Hybrid step motors introduced in Chapter 2 are efficient and compact step motor types. A hybrid step motor is implemented by stacking different rotor or stator poles on a single shaft. Motor size is reduced by allowing bipolar drive, i.e. the ability to excite motor windings in both directions. Bipolar excitation of a 2-phase hybrid step motor results in four distinct step pulses as shown in Figure 19 (a) where θ_s is the natural step angle. Winding currents of Phase-A and Phase-B follow the patterns given in Figure 19 (b).

Micro-stepping, discussed in Chapter 2 can increase the positioning precision and accuracy of the motor system by switching current from one phase to the other smoothly by subdividing natural steps of the step motor. The waveforms given in Figure 19 (b) can be converted to the sinusoidal forms as in Figure 19 (c) by micro-step excitation.

Micro-stepping *resolution* is the number of distinct excitation current configurations in a micro-stepping drive. In other words, it is the number of micro-steps in full electrical input pulse period, which contains four natural steps in bipolar drive of a 2-phase hybrid step motor. The number of micro-steps needed for one natural step, μ_s, of the motor is given by (9), where γ is the operation resolution.

$$\mu_s = \frac{\gamma}{4} \tag{9}$$

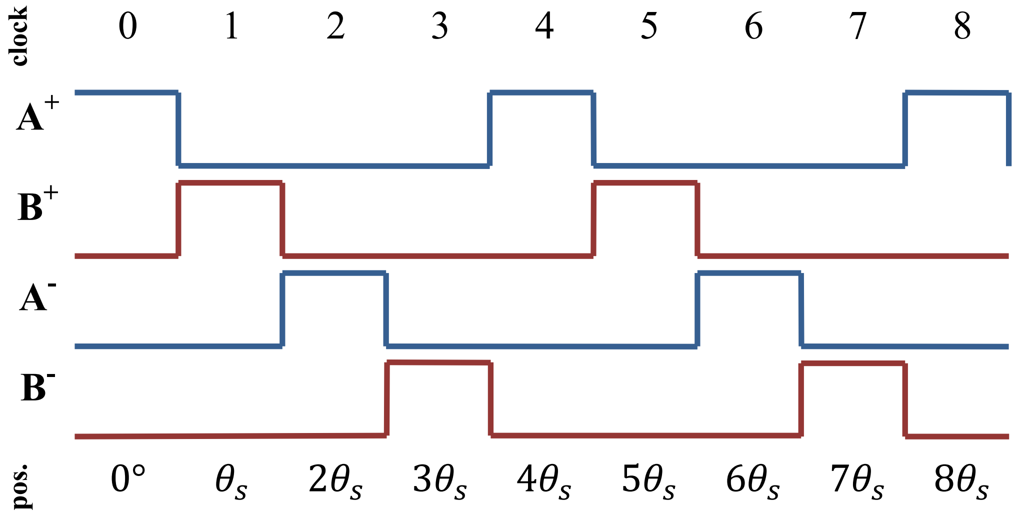

(a)

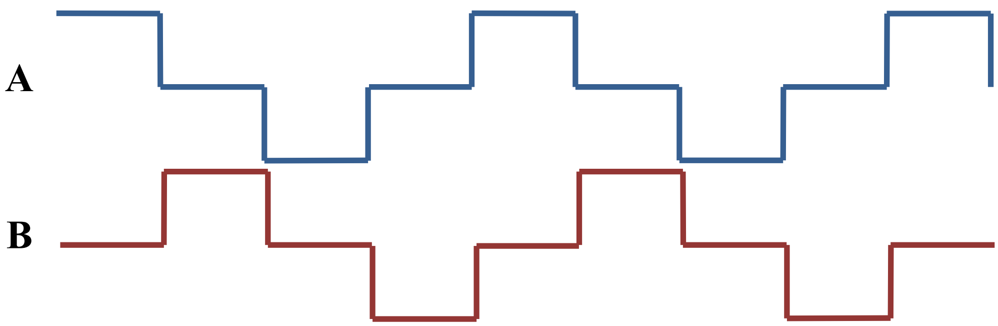

(b)

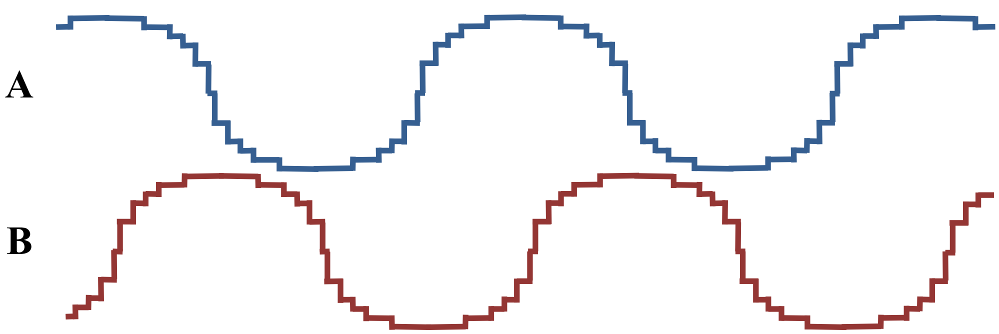

(c)

Figure 19 (a) Natural steps in bipolar drive of a 2-phase hybrid step motor. (b) Winding current waveform of both phases in bipolar wave drive and (c) bipolar micro-stepping excitation of the same motor.

Full-bridge converters for each phase of the motor control the amount and direction of the current flowing through the associated winding. Digital control and gate drivers supply the switching inputs for the transistors in full-bridge circuits.

4.2 Full-Bridge Converters

4.2.1 Topology and Operation

The full-bridge converter is a topology that allows winding current to flow in both directions and it is the typical driving circuitry for bipolar step motors. Full-bridge converter has two legs as shown in Figure 20. Each leg contains two switches and two anti-parallel diodes, also called *catch* diodes. The center points of the two legs are the output ports of the bridge and connected to the load. Full-bridge circuitry is also called *H-bridge.*

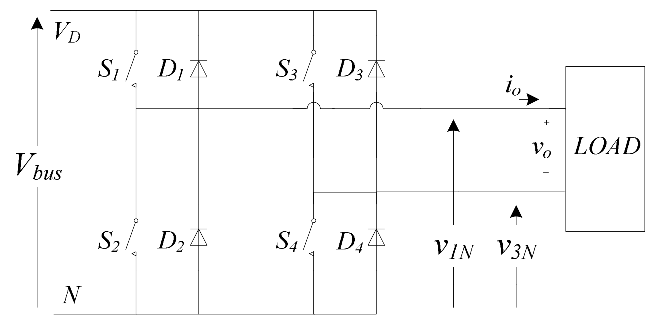

Figure 20 The full-bridge converter.

The output voltage is given in (10) with respect to the node voltages given in Figure 20. Each switch and its anti-parallel diode constitute a bi-directional path to the current to flow. Thus, v_{1N} and v_{3N} are independent of the polarity of the output current and they can be manipulated by only changing the state of the switches. The value of v_{1N} and v_{3N} can be expressed by (11) and (12).

$$v_o = v_{1N} - v_{3N} \tag{10}$$

$$v_{1N} = \begin{cases} V_{bus} & ; \quad S1 \text{ is conducting and } S2 \text{ is } OFF \\ 0 & ; \quad S2 \text{ is conducting and } S1 \text{ is } OFF \end{cases} \tag{11}$$

$$v_{3N} = \begin{cases} V_{bus} & ; \quad S3 \text{ is conducting and } S4 \text{ is } OFF \\ 0 & ; \quad S4 \text{ is conducting and } S3 \text{ is } OFF \end{cases} \tag{12}$$

The average values of v_{1N} and v_{3N} are given in (13) and (14) where $t1_{on}$ is the on time and $t1_{off}$ is the off time for $S1$, T_s is the full period time and D_1 is the duty ratio of $S1$. The mean value of v_o is found as in (15).

$$\overline{v_{1N}} = \frac{V_{bus} \cdot t1_{on} + 0 \cdot t1_{off}}{T_s} = V_{bus} \cdot D_1 \tag{13}$$

$$\overline{v_{3N}} = V_{bus} \cdot D_3 \tag{14}$$

$$\overline{v_o} = V_{bus} \cdot (D1 - D3) \tag{15}$$

4.2.2 Drive and Decay

The driver implemented in this thesis uses PWM chopping for driving the phase winding currents. PWM signals control the winding excitation of each phase where the duty cycle is proportional to the absolute value of the current waveform at a single micro-step. A full-bridge circuit for each phase ensures that during the on state of the PWM, phase windings are energized and during the off state phase currents decay.

An important issue to note is that conducting of both the switches in a single leg creates a short circuit between the voltage source and the ground and this must be avoided. To prevent this, an additional t_{off} time is introduced before one switch is turned on and after the other one is turned off. This time is called *blanking time* or *dead-time* and necessary for safe operation in cases where simultaneous switching is needed. In the analysis of v_o dead-time is neglected and it turned out to be directly proportional to the reference voltage selected. However, dead-time brings nonlinearity to the system and in a practical bridge, v_o formulation is more complicated than presented here.

One technique to drive the bridge is turning *S1* and *S4* on while turning *S2* and *S3* off as the first state, and in the second state turning *S2* and *S3* on while turning *S1* and *S4* off. This is achieved by giving complementary PWM signals to the gate drive circuitries of *S1*-*S4* and *S2*-*S3* switch pairs. In full-bridge terminology, this type of driving is referred as *bipolar driving mode*, and the PWM scheme is called *two-level PWM.* Bipolarity achieved because v_o changes between two output voltage levels, $+V_{bus}$ and $-V_{bus}$. Duration ratios of these two states are *D1* and *D3*, which determine the winding current from the average of voltage chopper introduced in Chapter 3.

Another PWM technique is called the *three-level PWM* scheme. This name indicates the $+V_{bus}$, $-V_{bus}$ and zero level of v_o can be obtained from (15). The third output state, $v_o = 0$, can be achieved when *S1* and *S3* are turned off while *S2* and *S4* are turned on or vice-versa. This mode allows a passive decay of the current inside the windings. Current in positive direction can be achieved by switching between $v_o = +V_{bus}$ and $v_o = 0$ states. Current in the opposite direction is achieved by switching between $v_o = -V_{bus}$ and $v_o = 0$ states.

One typical difference between two-level PWM and three-level PWM is the rate of change of output current, i_o during the operation. In two-level PWM scheme, i_o changes faster than the three-level PWM scheme. This allows higher PWM frequency in the expense of higher current ripple.

Several other different switching schemes can be applied on full-bridge converters besides two-level and three-level PWM [42,43]. One method is based on mixing these two schemes in order to benefit from the advantages of the two schemes to some extent. This method is called *mixed-mode PWM* [26].

In step motor terminology, different PWM techniques are referred as *decay modes* since they only differ in the switch configuration when the current inside the windings are decaying. Two-level PWM scheme is called *fast-decay*. Three-level PWM corresponds to a set of *slow-decay* modes. Slow-decay can be implemented in many ways. Some drive and decay modes are shown in Figure 21. The states in two-state PWM are shown in Figure 21 (a) and (b). In these states, $+V_{bus}$ and $-V_{bus}$ is applied to the motor windings respectively, thus one state can be used to decay the current driven by the other. Thus, a fast active decay occurs. Figure 21 (c), (d), (e) and (f) show different variations of slow decay implementation. In these operations, the motor winding is short circuited. All four of these examples show the decay current that is driven previously by the drive shown in Figure 21 (a). *Slow decay low mosfet re-circulation* as shown in Figure 21 (d) is used as the third PWM state in the step motor driver implemented in this thesis because *bootstrapping* occurs naturally during operation. Bootstrapping is the charging of gate driver capacitors and discussed in the next section.

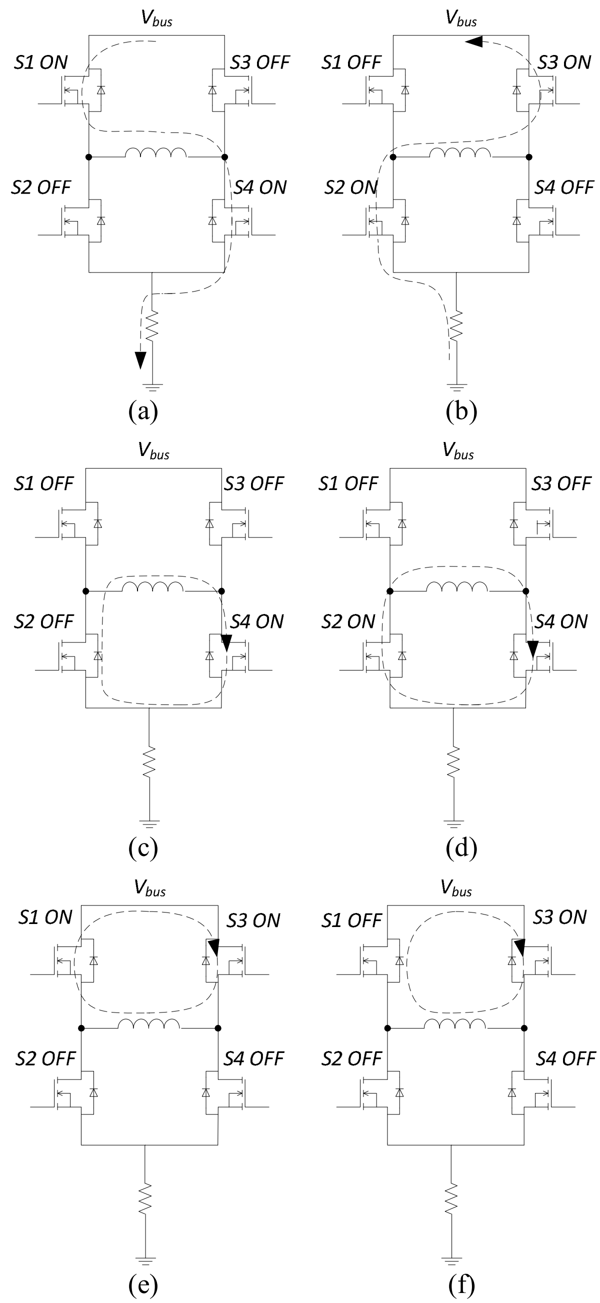

Figure 21 Full-bridge decay modes corresponding to different PWM states. (a) Drive with $v_o = +V_{bus}$ state and (b) its decay with $v_o = -V_{bus}$ state in two-state PWM. Different decay modes in three-state PWM: (c) slow decay low diode re-circulation, (d) slow decay low mosfet re-circulation, (e) slow decay high mosfet re-circulation and (f) slow decay high diode re-circulation.

4.2.3 Component Selection

Selection of the switching elements is a key issue. Controlled switching elements which are named as *S1* to *S4* in Figure 20 are generally realized as *MOSFET* or *IGBT.* These devices are preferable over *BJT*s for their ease of control mechanism. MOSFET's are voltage controlled devices having high input impedance. The gate current needed to turn on and off a MOSFET is small, whereas BJTs are current controlled devices and the base drive current requirement is a significant portion of the collector current. This makes MOS-gated devices, MOSFET and IGBT preferable for this application.

Selection between MOSFET and IGBT is made primarily according to the power requirement of the application. Typically MOSFET is preferred for applications with operating voltages up to several hundred volts and output power up to 500W. IGBT is more suitable for the operating ranges above 1000V and 5kW output power. Other conditions such as switching frequency or operating temperature are the deterministic features for the device selection for the operating area between these ranges. MOSFET is more preferable, for high frequency applications because MOSFETs have typically relatively shorter turn off times leading to a better transient characteristics. However, despite switching frequency is still the dominant feature, IGBTs become more preferable with lower switching frequencies for high operating temperatures [44]. As the proposed driver for this thesis is assigned to be below 100W, MOSFET selection criteria will be discussed hereafter.

Voltage and current ratings are basic parameters for power switching devices. The average voltage rating of MOSFET should be larger than the bus voltage in an H-bridge circuitry. An additional safety margin should be added considering the bus voltage variations or spikes originated from load side. There are typically two types of current ratings specified for switching devices, continuous current and the peak pulse current.

MOSFET acts as a resistor in on-state. R_{DSon} indicates the on-time resistance of the switch and this value greatly changes with temperature. This change can be calculated approximately with (16) where $R_{DSon(SPEC)}$ is the on-time resistance corresponding to the junction temperature $T_{j(SPEC)}$, and $R_{DSon(HOT)}$ is effective resistance when $T_{j(HOT)}$ is the operating temperature [45].

$$R_{DSon(HOT)} = R_{DSon(SPEC)} \cdot \left(1 + 0.005 \cdot \left(T_{j(HOT)} - T_{j(SPEC)}\right)\right) \tag{16}$$

Power dissipation on the device at on-time is referred as *conduction loss* and it is directly dependent on effective on-time resistance (17).

$$P_{diss_{on}} = R_{DSon} * (I_{DS})^2 \tag{17}$$

Selecting a device with low R_{DSon} is more preferable. However, there is a trade-off. Typically, as R_{DSon} gets smaller, the package of the device gets bigger [46]. This brings a new concern such that a bigger package size means a bigger gate and gate capacitance. Gate capacitance is a characteristic parameter that determines the t_{on}, turn-on time and t_{off}, turn-off time of the MOSFET gate. High gate capacitance leads to slower turn-on and turn-off gate, thus higher *switching loss*. Switching power dissipation is given in (18), where E_{on} and E_{off} are the values of dissipated energy during switching, turn-on and turn-off respectively, while f_{sw} is the switching frequency. E_{on} and similarly E_{off} can be approximated as in (19) in a hard switching case.

$$P_{diss_{sw}} = \left(E_{on} + E_{off}\right) \cdot f_{sw} \tag{18}$$

$$E_{on} \approx \frac{t_{on} \cdot V_{DS} \cdot I_{DS}}{2} \tag{19}$$

Parameters relating to the gate charge are more useful than internal capacitance values, C_{GD}, C_{GS} and C_{DS} for comparing switching characteristics of two different MOSFETs. These parameters are Q_g, total gate charge, Q_{gs}, gate-to-source charge and Q_{gd}, gate-to-drain charge and they provide an initial idea on the switching times with a simple calculation in (20).

$$Q_g = I_{gate} \cdot t_{on} \tag{20}$$

Selection of the uncontrolled switching elements, which are also named as *catch diodes* and are labeled as *D1* to *D4* in Figure 20, is done among power diodes and they are chosen usually as of Schottky type. These diodes carry current in the circuit when their anti-parallel switches are not conducting. The role of catch diodes becomes important especially for inductive loads. Being an inductive load, step motor builds an electromagnetic field inside the mechanical components during on-time. This field collapses when the switch is turned-off, but this cannot happen instantaneously. The current needs to flow through the load in the same way for some duration. Catch diodes provide a low resistance path for this current [46]. Thus, forward current capability of the diode should be equal to or greater than the rated current of the bridge.

One critical property of the diodes in a full-bridge converter application is the turn-on delay value. The load voltage forward biases the diodes to conduct after switches are turned-off. However, due to the gate capacitance of the diode, a turn-on delay is introduced. The load voltage can rise to levels that may damage the switching devices in this interval. Thus, turn-on delay should be as small as possible. *Ultrafast diodes* are preferred for this task.

Forward voltage drop of the diode is another important parameter. This value typically varies between 0.5V and 2V and it is intended to be small for power dissipation considerations. Power dissipation on the freewheeling diode can be approximated as in (21) by considering an ideal inductive load where V_f is the forward voltage drop on the diode and D is the on ratio of the diode in an off-cycle.

$$P_{diode} = \frac{I_{load} \cdot V_f \cdot D}{2} \tag{21}$$

Power dissipation on the diode becomes significant as the on ratio of the diode gets higher. This is related to the decay rate of the load current. If a duty ratio is selected for the bridge switch that does not allow the field current to decay to zero completely in the off-cycle, i.e. $D = 1$, power dissipation of the diode can become significant. In addition, power diode should have a reverse blocking voltage higher than the bus voltage.

In the light of these discussions, a MOSFET with a part name of *IRF640N* is selected as the controlled switching device [47] for this driver. Some parameters of the IRF640N are summarized in Table 1. MOSFET IRF640N body diode characteristics are given in IRF640N source-to-drain characteristics table, Table 2 separately. Utilizing the internal body diode of MOSFET as the freewheeling diode is an option. An ultrafast diode

MUR420 with better transient performance than the body diode of IRF640N MOSFET is selected for this driver [48]. Some parameters of the MUR420 are summarized in Table 3.

Table 1 Electrical characteristics of IRF640N.

V_{DSS}	Drain-to-Source Breakdown Voltage at V_{GS}=0Vand I_D= 250µA	200V
I_D	Continuous Drain Current at V_{GS}=10V and T_C=25°C	18A
I_D	Continuous Drain Current at V_{GS}=10V and T_C=100°C	13A
I_{DM}	Pulsed Drain Current	72A
$R_{DS(on)\ MAX}$	Static Drain-to-Source On-Resistance at V_{GS}=10V, I_D=11A	150mΩ
$V_{GS(th)\ MAX}$	Gate Threshold Voltage at V_{DS}=V_{GS} and I_D=250µA	4V
V_{GS}	Gat -to-Source Voltage	± 20V
Q_g	Total Gate Charge at I_D=11A, V_{DS}=160V and V_{GS}=10V	67nC
Q_{gs}	Gate-to-Source Charge at I_D=11A, V_{DS}=160V and V_{GS}=10V	11nC
Q_{gd}	Gate-to-Drain Charge at I_D=11A, V_{DS}=160V and V_{GS}=10V	33nC
t_r	Rise Time at V_{DD}=100V, I_D=11A, R_{GATE}=2.5Ω and R_{DRAIN} =9Ω	19ns
$t_{d(on)}$	Turn-on Delay at V_{DD}=100V, I_D=11A, R_{GATE}=2.5Ω, R_{DRAIN}=9Ω	10ns
t_f	Fall Time at V_{DD}=100V, I_D=11A, R_{GATE}=2.5Ω and R_{DRAIN} =9Ω	5.5ns
$t_{d(off)}$	Turn-off Delay at V_{DD}=100V, I_D=11A, R_{GATE}=2.5Ω, R_{DRAIN} =9Ω	23n

Table 2 Source-drain ratings and characteristics of IRF640N.

I_S	Continuous Source Current (Body Diode)	18A
I_{SM}	Pulsed Source Current (Body Diode)	72A
V_{SD}	Diode Forward Voltage at I_S=11A, V_{GS}=0V	1.3V
$t_{rr\ MAX}$	Reverse Recovery Time at I_F=11A and *di/dt*=100A/µs	251ns
$Q_{rr\ MAX}$	Reverse Recovery Charge at I_F=11A and *di/dt*=100A/µs	1394nC
I_S	Continuous Source Current (Body Diode)	18A

Table 3 Electrical characteristics of MUR420.

$I_{f(AV)}$	Average Rectified Forward Current at T_A=80°C	4A
V_{RRM}	Peak Repetitive Reverse Voltage	200V
V_f	Maximum Instantaneous Forward Voltage at I_f=3A, T_J=150°C	0.71V
t_{rr}	Maximum Reverse Recovery Time at I_f=1A, di/dt=50 A/µs	35ns
t_{fr}	Maximum Forward Recovery Time at I_f=1A, di/dt=100 A/µs	25ns

4.2.4 Simulation

Before constructing the circuitry, the H-bridge circuit is simulated using a computer simulation package program, Ansoft Simplorer V7.0. [49].

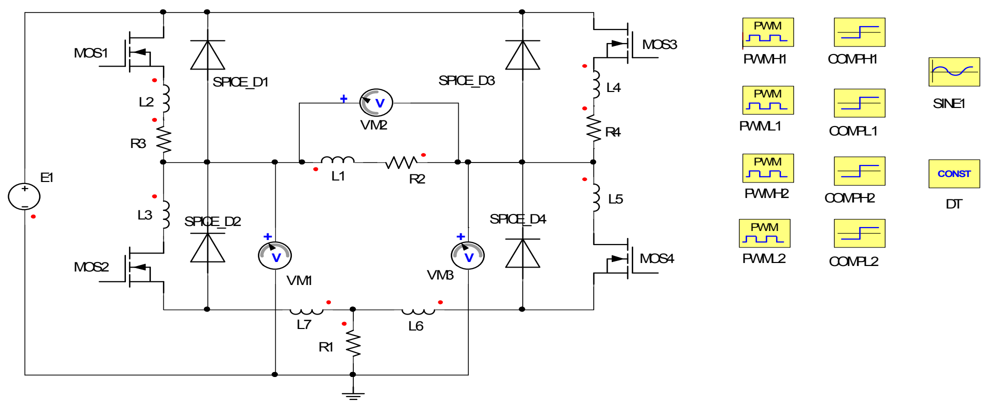

Figure 22 Simplorer schematic of full-bridge circuit.

In simulation, the motor is regarded as a series L-R circuit and back EMF is neglected for simplicity. Some parasitic elements, namely **L2**, **L3**, **L4**, **L5**, **L6**, **L7**, **R3** and **R4**, are added. The control signals for the MOSFET switches are in *value* format and created via math and time blocks in the simulation tool. Duty cycle variable of each PWM block is fed with its corresponding **COMP** block output which takes the related portion of the sinusoidal signal (output of the **SINE1** block), add dead-time (output of the **DT** block) and takes its absolute value. These signals are shown in Figure 23.

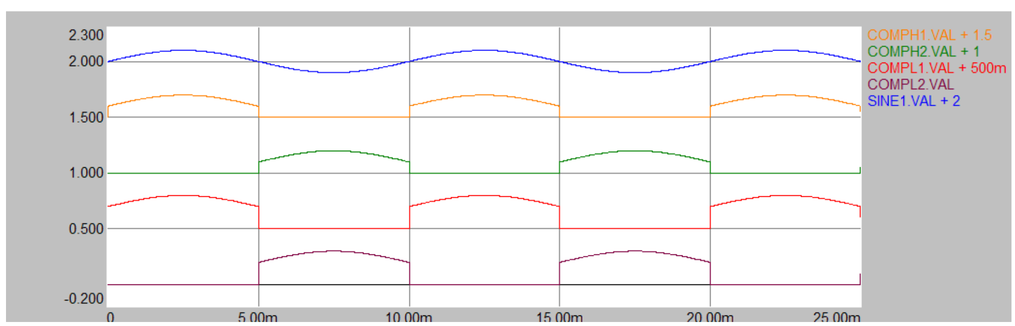

Figure 23 Duty cycle inputs of PWM blocks.

Bus voltage is selected as **E1** = 30V. Switches of the H-bridge circuit are exposed to this voltage and waveforms of voltage waveforms on **SPICE_D1-SPICE_D2** and **MOS1-MOS2** can be seen Figure 24 and Figure 25, respectively.

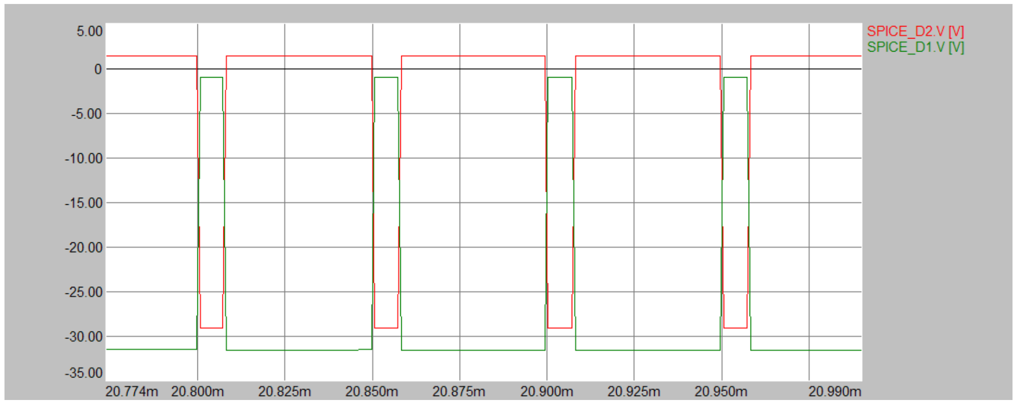

Figure 24 Voltage waveforms on SPICE_D1 and SPICE_D2.

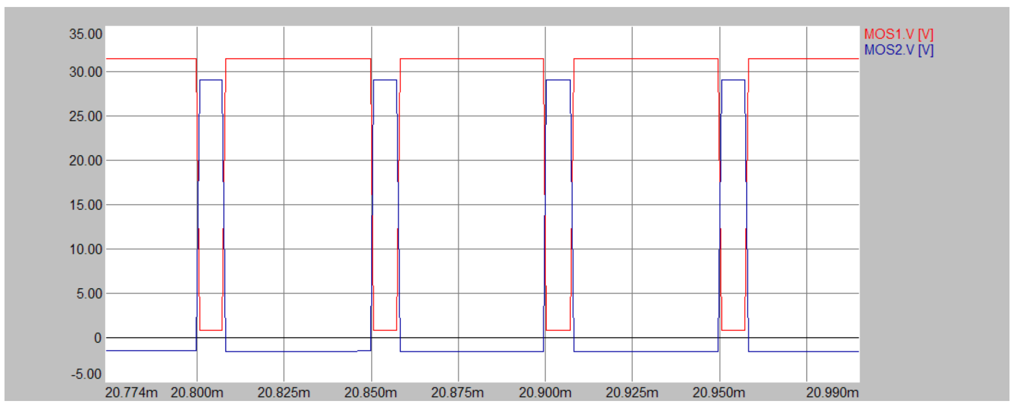

Figure 25 Voltage waveforms on MOS1 and MOS2.

Motor current and voltage waveforms are shown in Figure 26 while voltage and current waveforms on the sensing resistor **R1** = 0.1Ω are in Figure 27. Voltage and current waveforms on the sensing resistor are in a pulsed form, since in slow decay low MOSFET recirculation mode, only the drive current flows through this resistor. Decay current re-circulates over the motor and low-side switching elements. This brings a challenge to the evaluation process of the sensing current. Especially considering the cases where a high bus voltage is used in order to manipulate the current quickly, duty cycle on-time becomes small.

Rapid voltage and current changes occur due to the nature of the chopper configuration. Thus, there is a potential risk of observing unwanted signals on the sensing resistor that occurs right after the starting of the on-time originated from ground bounce issues. To overcome this problem, one solution can be taking the voltage sample from the sensing resistor when the waveform settles to the exact value after the effect of ground bounce is ended. Some series of processors from Microchip offer ADC capture for sensing current measurement after each PWM period beginning with an arrangement called *special event trigger* with a programmed delay value. By this way, the needed current sample can be provided from the pulsed and non-ideal waveform. Alternatively, the circuit configuration can be changed slightly so as to take the current waveform in a continuous manner. In this alternative configuration, the anodes of low-side freewheeling diodes are connected to ground instead of the upper node of the current sensing resistor. Thus, decay mode current also flows through sensing resistor. The pulsed waveform which is shown in the simulation results in Figure 27 changes to continuous form in the shape of the envelope of the former waveform. This waveform is easier to process. Moreover, it is now possible to close the current loop without using a complex digital processor.

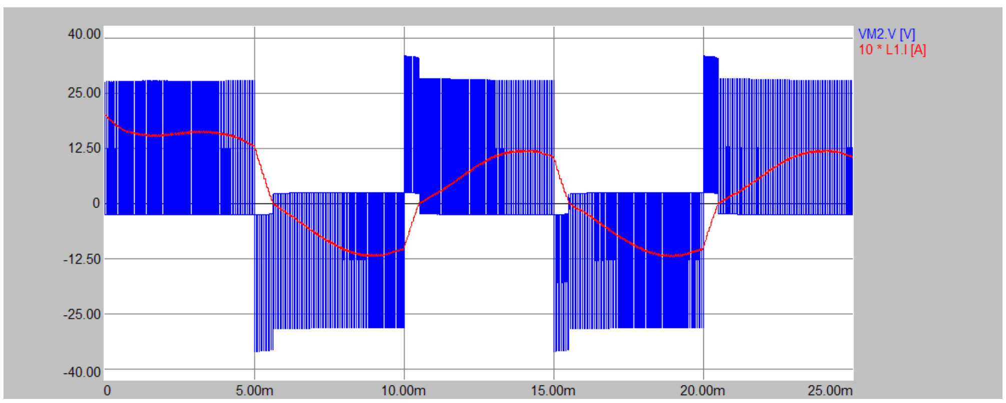

Figure 26 Voltage and current waveforms on the motor model.

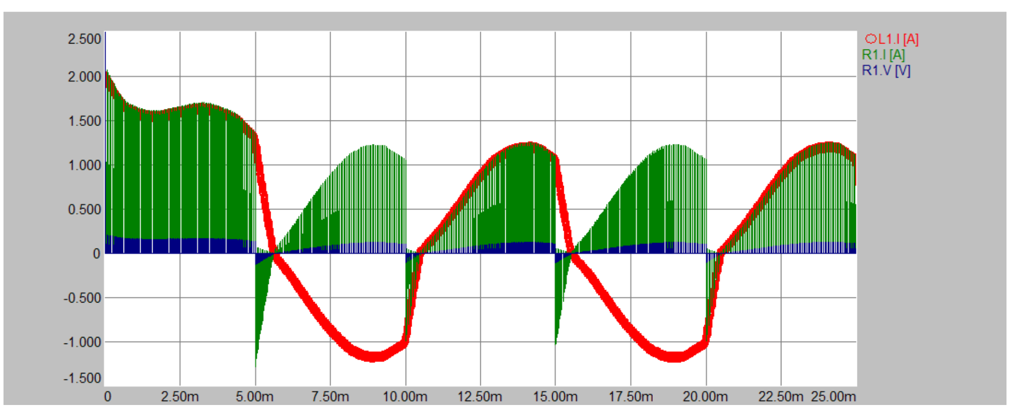

Figure 27 Sensing resistor voltage and current waveforms.

4.3 Gate Drivers

Gate driver circuit is the interface between the signal processing unit that generates the required logic levels and the MOSFETs. It does the amplification of these logic levels to the needed gate drive signals for the power switches. There may be some additional requirements based on the application such as isolation and timing issues.

High side and low side drivers are the two fundamental categories of gate drivers [50]. In a half bridge topology, there is one low-side and one high-side switch. The critical part of drive circuitry of an H-bridge is the drive of the high-side switch, since the gate voltage of a high-side switch is referenced to a floating ground other than the system ground. There should be an isolated ground in the system and source voltage of the high-side switch should be level shifted to this floating ground.

The gate voltage of the switch is probably the highest voltage found in the system [51] for a half bridge circuit constructed with N-channel MOSFETs, being typically 10-15V above the source voltage.

There are different drive methods that can be applicable to high-side switches such as charge pump drivers, pulse transformers as gate drive, secondary isolated power supplies or bootstrap drive circuits. Each drive method has its own advantages and disadvantages. For example, pulse transformers are ineffective for high switching frequencies due to the parasitics introduced by the transformer and as the frequency decreases, the transformer gets more bulky. Charge pump drivers are also not proper for the high frequency applications if the high side drive is provided by pumping the gate when the high-side switch is turned on [51]. Level shifting has its own difficulties which most of the configurations mentioned are subject to. First of all, the high-side reference voltage level is required to be constant. Also, meantime minimal switching times must be achieved to build a driver with a good performance. Secondary power supply brings a significant additional cost to the system. And lastly, bootstrap configuration has constraints related to the duty cycle and on-time of the high-side switch.

In this thesis, *IR2110*, a MOS-gate driver IC from International Rectifier is used [32]. Selected parameters among electrical characteristics of IR2110 are summarized in Table 4 and some of the absolute maximum ratings are given in Table 5.

Table 4 Electrical characteristics of IR2110.

$V_{IH\ MIN}$	Logic-1 input voltage at V_{DD}=V_{CC}=15V, V_{SS}=0V	9.5V
$V_{IL\ MAX}$	Logic-0 input voltage at V_{DD}=V_{CC}=15V, V_{SS}=0V	6.0V
$V_{OH\ MAX}$	High level output voltage at V_{DD}=V_{CC}=15V, V_{SS}=0V, I_o=0A	16.2V
$V_{OL\ MAX}$	Low level output voltage at V_{DD}=V_{CC}=15V, V_{SS}=0V, I_o=0A	0.1V
$V_{BSUV-\ MAX}$	VBS supply under-voltage negative going threshold	9.4V
I_{LK}	Offset supply leakage current	50µA
I_{QBS}	Quiescent V_{BS} supply current	230 µA
$t_{on\ MAX}$	Turn-on propagation delay at V_{SS}=V_S=0V, C_L=1000pF	150ns
$t_{off\ MAX}$	Turn-off propagation delay at V_S=500V, C_L=1000pF	125ns
$T_{SD\ MAX}$	Shut-down propagation delay at V_S=500V, C_L=1000pF	140ns
t_r	Turn-on rise time at V_S=500V, C_L=1000pF	35ns
t_f	Turn-off fall time at V_S=500V, C_L=1000pF	25ns
MT	Delay matching of high-side and low-side during turn-on and off	10ns

Table 5 Absolute maximum ratings of IR2110.

V_B	High side floating supply voltage	(-0.3V) – (525V)
V_{CC}	Low side fixed supply voltage	(-0.3V) – (25V)
V_{DD}	Logic supply voltage	(-0.3V) – (Vss + 25V)
Vss	Logic supply offset voltage	(V_{CC} - 25V) – (V_{CC} + 0.3V)
V_{IN}	Logic input voltage (HIN, LIN & SD)	(V_{SS} - 0.3V) – (V_{DD} + 0.3V)

High side switching can be achieved by using an isolated power supply or a bootstrap configuration by utilizing this integrated circuit. In this application, bootstrap configuration is chosen where a few external components called *bootstrap components* are added to the driver circuit. These components are shown in Figure 28 as C_{BOOT} and D_{BOOT}. Bootstrap capacitor can be used instead of the isolated power supply of the high-side MOS-gated switch, since MOS type gates need a certain amount of gate charge to be turned on instead of continuous current as in the case of BJTs as discussed before. This capacitor is charged by V_{CC} through bootstrap diode.

As mentioned before, the basic limitation of bootstrap drive scheme is related to the duty cycle and on-time of high-side switches. This limitation stems from the charging issues of bootstrap capacitor. For a proper operation, bootstrap capacitor should be charged initially and remain charged during operation. When Q_L is turned-on in Figure 28, the source terminal of Q_H is at V_{DSon} potential which is near to ground potential. Q_H cannot be turned-on meantime in order not to short circuit the bus voltage. The charging path of C_{BOOT} which is shown in Figure 28 is open in this case. When Q_L is turned-off and Q_H is turned-on, the source terminal of Q_H begins to rise and C_{BOOT} provides gate current to turn the Q_H on. If high-side switch is left open indefinitely, bootstrap capacitor eventually discharges. In such a situation, bootstrap capacitor charge needs to be refreshed. Thus, to avoid such situation, duty cycle of the high-side switch should be limited. Capacitor sizing is critical to overcome these limitations to some extent.

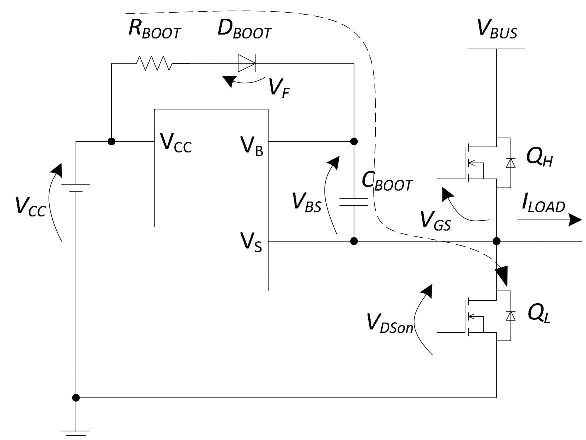

Figure 28 Bootstrap configuration for IR2110.

Selection criteria for bootstrap capacitor are discussed in [52]. First step to choose the value of the bootstrap capacitor is given as calculating the voltage drop on V_{BS} voltage in a state where turning on Q_H is guaranteed. The maximum allowed V_{BS} voltage drop value, ΔV_{BS}, where high-side switch can still be controlled by C_{BOOT} can be estimated by using (22), under the condition of (23). In these equations, V_{CC} is low-side driver fixed supply and is selected as 15V for this driver, V_F is the forward voltage drop of D_{BOOT} and $V_F = 1.7$V [53] and V_{DSon} is the voltage drop on the low-side switch when it is on and it can be found by (24) as $V_{DSon} = 0.3$V for $I_D = 2$A.

$$\Delta V_{BS} \leq V_{CC} - (V_F + V_{GSmin} + V_{DSon}) \tag{22}$$

$$V_{GSmin} > V_{BSUV-} \tag{23}$$

$$V_{DSon} = R_{DSon} \cdot I_D \tag{24}$$

V_{GSmin} is the minimum gate to source voltage that is sufficient to turn-on the high-side switch. According to IRF640N data sheet, $V_{GS} = 5V$ is the corresponding gate to source voltage for $I_D = 2A$ [47]. However, (22) is valid under the condition of (23). Thus, V_{GSmin} is selected as $V_{BSUV\text{-}MAX}$ value of IR2110 driver [32], and $V_{GSmin} = 9.4V$. ΔV_{BS} is found to be 3.6V in this case.

The next step to calculate C_{BOOT} value is to list the factors that cause V_{BS} to decrease. These are:

- Q_g, total gate charge of high-side FET:
  $Q_g = 67nC$ (as stated in Table-1 IRF640N Electrical Characteristics)
- Q_{ls}, level shift charge required per cycle:
  Typical values are given in [51] as 5 nC for 500 V/600 V driver ICs
- $I_{cbs(leak)}$, leakage current of C_{BOOT}:
  This value is not significant and can be neglected if ceramic capacitors are utilized alone or paralleled with another type of capacitor.
- I_{LK}, floating section leakage current :
  $I_{LK} = 50\mu A$ (as stated in Table-4 Electrical Characteristics of IR2110)
- I_{QBS}, floating section quiescent current:
  $I_{QBS} = 230\ \mu A$ (as stated in Table-4 Electrical Characteristics of IR2110)
- T_{Hon}, high-side on time:
  D_{on} is limited to 0.8 in this application. For $f = 32kHz$, $T_{Hon} = 25\mu sec$.

By using these parameters, total charge that V_{BS} should supply is calculated by using (25) as 79nC.

$$Q_{TOT} = Q_g + Q_{ls} + (I_{cbs(leak)} + I_{LK} + I_{QBS}) \cdot T_{Hon} \tag{25}$$

Minimum C_{BOOT} value is given in (26).

$$C_{BOOT\_MIN} = \frac{Q_{TOT}}{\Delta V_{BS}} = \frac{79nC}{3.6V} = 22\text{nF} \tag{26}$$

UF4007 is suitable for D_{BOOT} with a fast recovery time (t_{rr} = 75ns). A blocking voltage higher than V_{BUS} is selected.

Another important issue about the H-bridge topology is adding a dead-time between high-side and low-side switches to avoid short circuiting the bus voltage. IR2110 introduces an approximately 25ns dead-time as a consequence of close mismatch of propagation delays where worst case MT is stated as 10ns and turn-on propagation delay being 25ns longer than turn-off propagation delay. To add a safety margin, a resistor-diode network is added to the gate [51]. The effect of this network is further delaying the turn-on, without changing the turn-off time.

4.4 Digital Control

4.4.1 Microcontroller

All the digital domain operations are accomplished on a microcontroller. These are interpreting the input commands coming from the controller unit, storing the current reference table, managing the current control calculations utilizing ADC channels or alternatively, analog comparator outputs and generating the PWM signals accordingly.

PIC18F4431 [31] is selected for this task. PIC18F4431 is an 8-bit microcontroller that can be operated at up-to 40MHz with external oscillator and is preferable due to its features that are useful for motor control applications, such as advanced PWM, A/D modules and encoder interface.

4.4.2 Scope and Specifications

The first task according to the operation sequence is interpreting the input commands. These are step and the direction input. Step input comes in a pulse form, where negative edge of the each active low pulse represents a command for a new step. Direction input is in binary format, where one represents clockwise direction, and zero represents a counter-clockwise direction. Waveform diagrams of these input signals are shown in Figure 29.

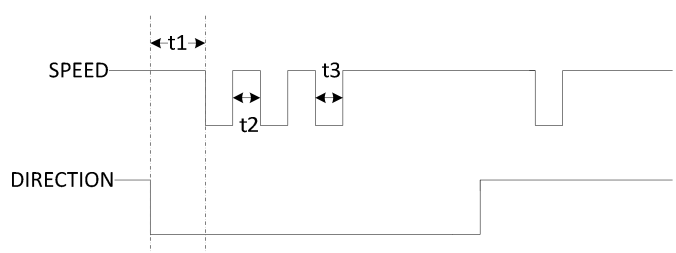

Figure 29 Timing diagram of input commands.

These two signals are generated in the controller unit and conditioned in an opto-coupler circuitry which is shown in Figure 30. This circuit provides isolation between controller unit and driver, and also filters input spikes with proper *R_IN* and *C_IN* values. *t2* is restricted by the input filter time constant which is given in (27) and is expected to be about ten times of this value. *t1* and *t3* are restricted by the microcontroller speed.

$$\tau = R\_IN * C\_IN \tag{27}$$

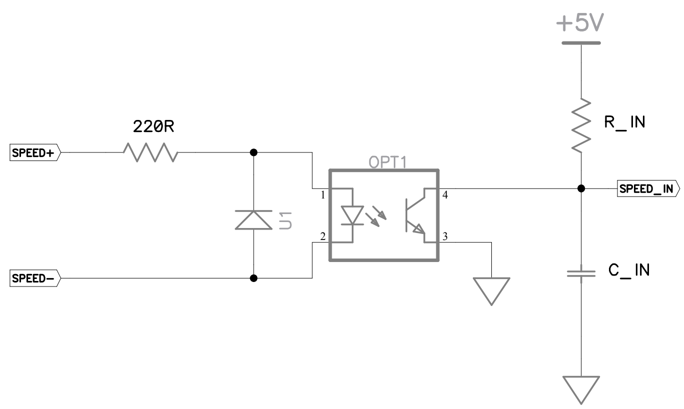

Figure 30 Opto-coupler circuit for input command.

Step input is connected to one of the timer inputs of the microcontroller check at every PWM period beginning along with the direction input.

A/D interface is capable of simultaneously processing two ADC inputs at a time and sequential sampling is possible. A/D module is triggered by the power control PWM period beginning. Acquisition time of the A/D module is programmable.

PWM outputs are generated by using the power control PWM module which simplifies generation of the needed gate signals for half-bridge switches by utilizing the available complementary mode and programmable dead-time generator.

PWM signals are controlled over a digital counter inside the microcontroller. PWM outputs are generated by comparing this counter, *ptmr*, with the reference duty cycle value d_{PWM}

according to the formula given in (28), where *CS1* is the appropriate drive signal that controls gate voltages of upper full-bridge transistors and *CS2* is its inverse.

$$\begin{aligned} CS1 = 1, CS2 = 0 \quad &; d_{PWM} \geq ptmr \\ CS1 = 0, CS2 = 1 \quad &; d_{PWM} < ptmr \end{aligned} \tag{28}$$

The on time of *S1*, t_{on}, can be expressed in terms of the newly introduced parameters in (29) and [50] where p_{PWM} is the PWM period value and the maximum of *ptmr* where *ptmr* drops to zero when reached to p_{PWM}. Duty ratio of *S1* is also revealed with (30).

$$t_{on} = \frac{d_{PWM}}{p_{PWM}} \cdot T_s \tag{29}$$

$$D1 = \frac{t_{on}}{T_s} = \frac{d_{PWM}}{p_{PWM}} \tag{30}$$

Thus *D1* and *D3*, and therefore also *D2* and *D4* can easily be controlled by adjusting the duty cycle and period values inside the microcontroller. This results in a complete control of all available v_o levels.

4.4.3 Algorithm

The microcontroller runs an interrupt driven software program where the most critical operations are handled in an interrupt handler routine. The execution is switched to the interrupt routine when *ptmr* resets to zero and a new PWM period begins. Figure 31 shows the summary of the software code that generates the PWM signals for driving the step motor.

The microcontroller performs initialization tasks on reset. Firstly, pin control registers are set to enable correct communication between microcontroller and the peripherals. Afterwards, several variables and flags are reset to their default values. This includes setting the iteration index for current micro-step to the beginning of a *look-up table* that is stored inside the *electrically erasable programmable read-only memory* (EEPROM) of the microcontroller. This table stores PWM duty cycles for every possible micro-step and its contents are calculated offline on a desktop computer.

Controller inputs, which are direction and step pulse, are connected to two different digital input pins of the microcontroller. The direction input is continuous and thus it is polled periodically. Step pulse input is a short logical pulse that is sent by the controller to request a single micro-stepping rotation in the direction dictated by the direction input. Pulse input is collected asynchronous from the instruction execution with the external counter capabilities of microcontroller timer. A periodic check on this counter ensures capture of pulses even if they end before the check.

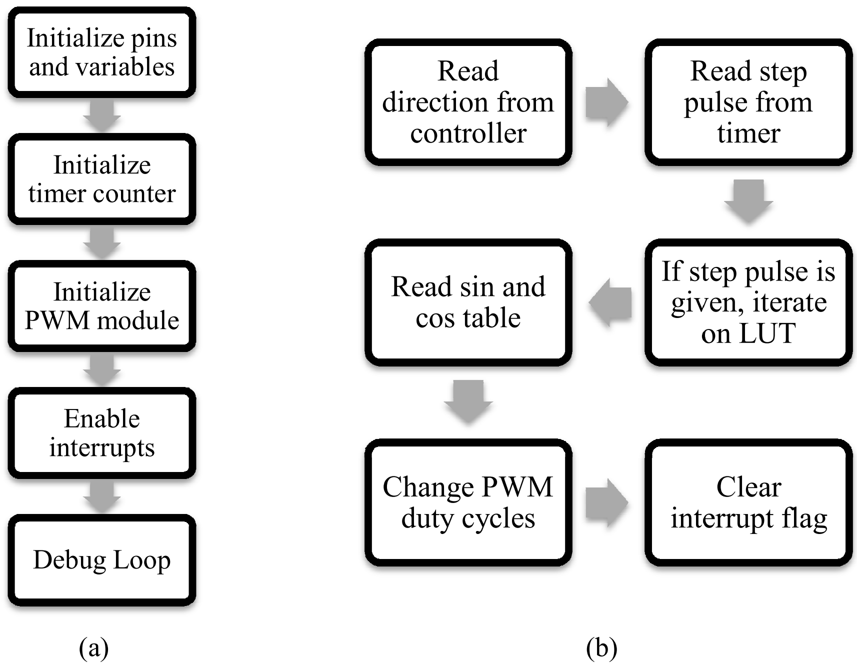

Figure 31 Flowcharts for (a) Main execution and (b) interrupt routine for microcontroller software.

The PIC18F4431 features a power PWM module that supports eight PWM outputs with output complementary modes, programmable dead-time insertions and optional PWM override with logical levels. Eight PWM pins are connected to the eight gate driver inputs to drive eight transistors contained in two full-bridge converters for two phases. The PWM pins are run in complementary mode where even numbered PWM pins output the inverse of their odd numbered counterparts with possible dead-time insertions. Odd numbered pins are connected to high side transistors and low side transistor gates are always fed with the inverse PWM signals. PWM module is also configured to raise interrupts when *ptmr* changes to zero.

Initialization on microcontroller reset ends with the enabling of system-wide interrupts. This starts the periodic call of the interrupt handler when PWM periods begin. After initialization, the main execution switches to a continuous debug loop where variables in the code are sent to some digital output pins serially at low speeds. This is only used to trace and confirm correct operation of the software during development stage.

The system automatically increments *ptmr* at every clock of the external oscillator connected to the microcontroller. When *ptmr* exceeds p_{PWM}, it is reset back to zero and an interrupt flag is set to break main execution and switch instruction flow to an interrupt handler at the first opportunity. The actual work of the microcontroller is done inside this interrupt handler.

The interrupt handler routine starts with the polling of controller commands. Direction input is read directly from the connected input port and the step pulse is read from an externally incremented counter value. If this counter contains a value and clockwise direction is requested, the iterator index on sinusoidal look-up table is incremented. If counter-clockwise direction is requested this index is decremented.

The table index, whether it is modified or not, stores the duty cycle to use for the current micro-step for the first phase. The duty cycle for the second phase can be found by fetching from the table with an offset corresponding to 90º, e.g. an offset of 32 is used for a micro-step resolution of 128. These duty cycles are written to duty cycle registers of the microcontroller to take effect starting from the next PWM period. Delaying of duty cycle change is possible with the double buffering features of power PWM module.

The interrupt routine ends by clearing the interrupt flag which caused the handler to execute. This ensures the handling of further requests if necessary.

The software for the microcontroller is written in *C* and compiled to chip binary with HI-TECH Picc18 compiler of *Microchip Technology*.

4.5 Current Control Feedback

Current reference table stored inside the EEPROM of the microcontroller keeps reference current values for micro-stepping operation. A pulse counter is incremented for each step input when direction is positive and decremented when direction is negative. This counter is used as an index for the current reference table. So, referent current value is refreshed based on this information. The output of the driver is forced to follow the reference current by means of the power converter components described earlier.

There are two approaches to control current in step motor drives [27] in a loop. First approach is to use an ADC to convert measured analog current to digital and compare this current value with the referent current in digital domain. In second approach, referent current is converted to analog by using a DAC and the comparison is done in analog domain by means of a comparator.

The implemented driver supports both current control mechanisms and it can switch from one to another with its microcontroller software. The ADC measurement approach is supplemented with a PI control software block which performs tuning of duty cycle values with respect to the PI output as described in Chapter 3. The DAC approach leads to a simple P control where appropriate gate drivers are shutdown when the control error is negative.

CHAPTER 5

EXPERIMENTS

Conducted experiments to test the operational validity and performance of the designed step motor driver are explained in this chapter. The chapter starts with an introduction of the experimental setup in the first section. Then, tests relating to validation of the operation of the motor driver are presented. Finally, test results of the implemented driver with a CNC controller for its performance on accuracy and torque output are discussed.

5.1 Experimental Setup

The designed step motor driver is implemented on a four layer *printed circuit board* (PCB) as seen in Figure 32. Also, an accompanying test setup composed of a controller with user input panel and a power stage that provides 34V DC supply from 220V AC input has been established for the tests of the step motor driver designed and implemented in this thesis.

User input contains power on/off switch and direction input switches, a POT as the adjustable step input and a button to start and stop motion. The setup is shown in Figure 33.

Table 6 Step motors tested for driver operation.

Motor Type	*Specifications*
57SH-46N2C	5 deg/rev, R=0.94Ω/phase
23LM C058-05H	1.8 deg/rev, 1.4A/phase, 3.5V/phase
103G770-3441	1.8deg/rev, 1.35A, 3.9V

Several two-phase bipolar hybrid step motors are used in the tests. The names of these motors are given in Table 6 with their specifications.

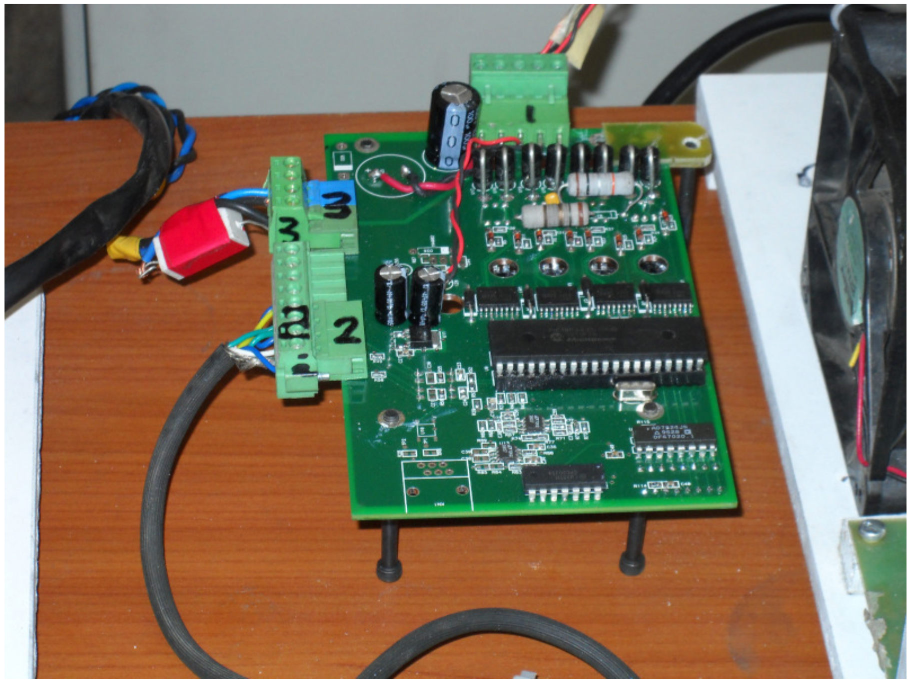

Figure 32 Implemented step motor driver on PCB.

Figure 33 Experimental setup: step motor and load on the left, driver in the middle and the power supply on the right. PC controller interface is seen in the front.

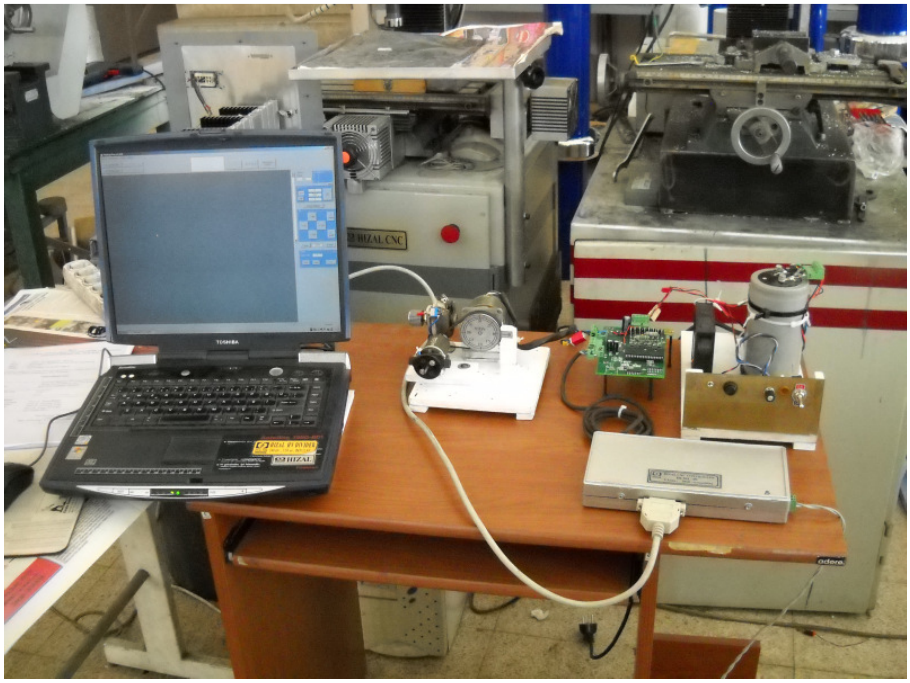

Figure 34 Laboratory test setup with controller PC on the left and two different controller interfaces on the right. The CNC drilling machine to operate is shown on the upper right corner.

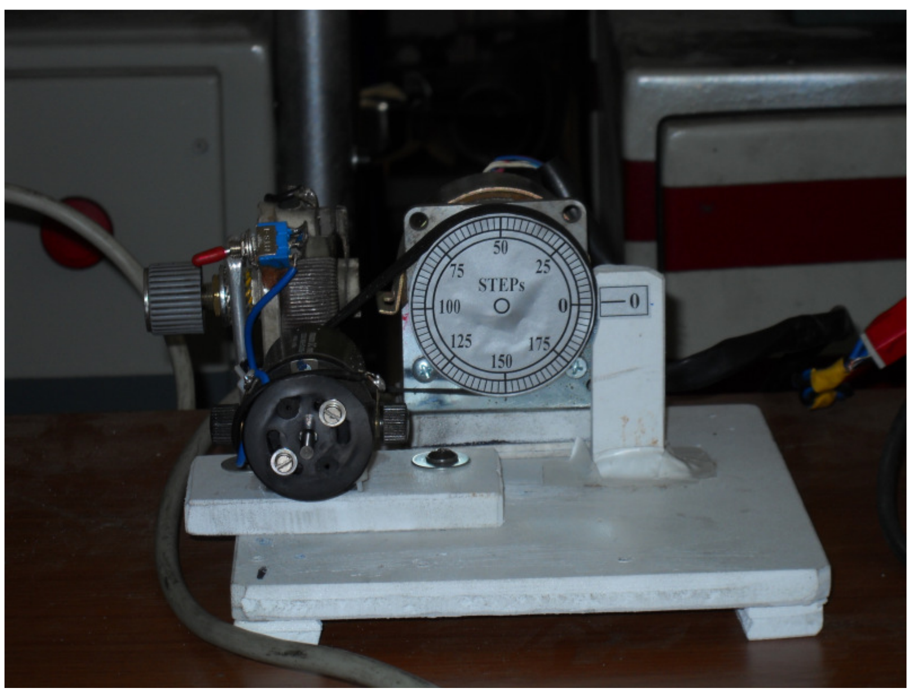

Figure 35 Setup for positioning tests.

Also, a DC motor with a type number of MAXON 2332.968-201 is used as a load generator for the test step motor. The DC motor shaft is matched to the shaft of the test motor with a flexible belt and the DC motor is operated in generator mode with a potentiometer connected across the wires of the DC motor to adjust the load of the test motor.

5.2 Waveform Measurements

Step motor driver is tested under different speed, current set-point conditions and micro-step resolutions. A *Tektronix TDS5104* digital oscilloscope with two *TCPA300* current probes is used for the measurements. The results are shown in Figure 36, Figure 37 and Figure 38.

Figure 36 (a) shows the clockwise and Figure 36 (b) shows the counter-clockwise operation when the desired current set-point is 500mA peak, micro-step resolution is 128 and shaft speed is 20rpm. The measurements are taken under no load condition.

Figure 36 (c) shows the current waveforms when a fixed load is connected to this configuration. Here, motor is still capable of positioning without error, but there is a slight distortion on the shape of current waveforms.

Figure 37 (a) shows the phase current waveforms when the desired current set-point is 800mA peak, micro-step resolution is 64 and shaft speed is 40rpm at no load. Since micro-stepping resolution is halved, rotor displacement corresponding to one step command is doubled. As a result, the speed of the rotor shaft is doubled with the same controller output pulse settings. The shapes of the current waveforms are smoother as a result of increased set current value. Figure 37 (b) shows the waveforms for the same configuration under a fixed load. On the other hand, Figure 37 (c) still provides the no load waveforms, but this time, step input rate from controller panel is increased. It can be observed that the peak current value that the phase currents can reach is lower due to the increased back-EMF voltage as the rotor speed increases from 40rpm to 54rpm.

Finally, Figure 38 (a) and (b) presents the current waveforms under no load and fixed load conditions when micro-step resolution is reduced to 8. In no load condition, test motor is able to start and stop properly. However, it loses steps with the same conditions under load. This is expected as the current waveform in this case varies radically from the wave drive pattern given in Figure 19 (b).

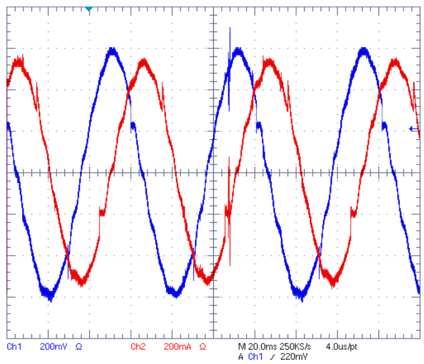

Current set-point	500mA
Micro-stepping resolution	128
Shaft speed	20rpm
Direction	CW
Load	None

(a)

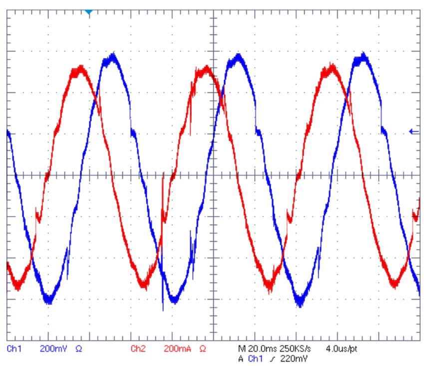

Current set-point	500mA
Micro-stepping resolution	128
Shaft speed	20rpm
Direction	CCW
Load	None

(b)

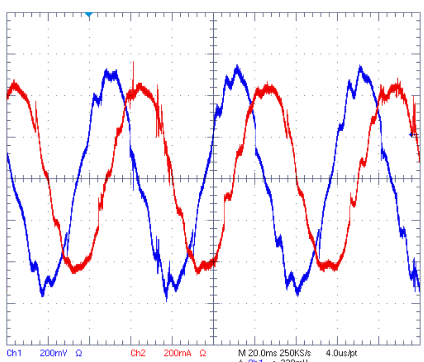

Current set-point	500mA
Micro-stepping resolution	128
Shaft speed	20rpm
Direction	CCW
Load	Fixed

(c)

Figure 36 Phase current waveforms for 128 micro-step resolution. Blue is phase-A and red is phase-B. (a) Clockwise rotation under no load, (b) counter-clockwise rotation under no load and (c) counter-clockwise rotation under fixed load.

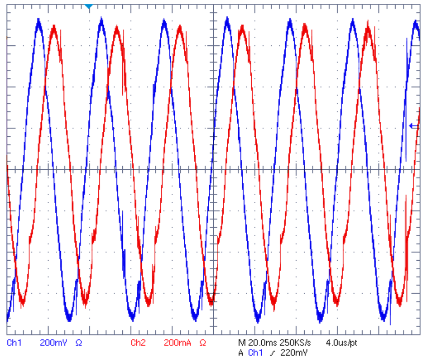

Current set-point	800mA
Micro-stepping resolution	64
Shaft speed	40rpm
Direction	CW
Load	None

(a)

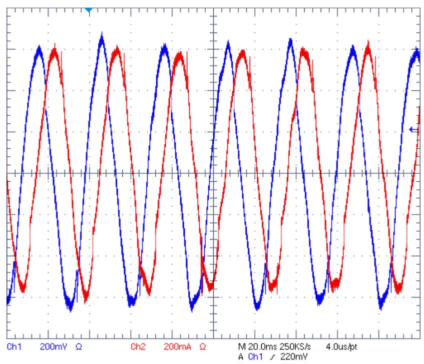

Current set-point	800mA
Micro-stepping resolution	64
Shaft speed	40rpm
Direction	CW
Load	Fixed

(b)

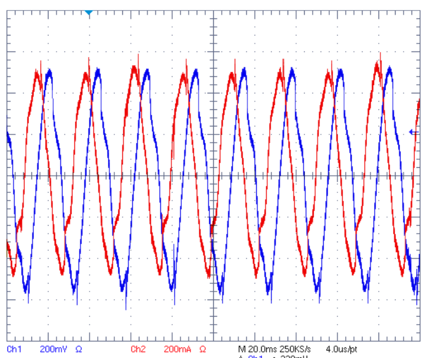

Current set-point	800mA
Micro-stepping resolution	64
Shaft speed	54rpm
Direction	CCW
Load	Fixed

(c)

Figure 37 Phase current waveforms for 64 micro-step resolution. Blue is phase-A and red is phase-B. (a) 40rpm speed under no load, (b) 40rpm speed under fixed load and (c) 54rpm speed under load.

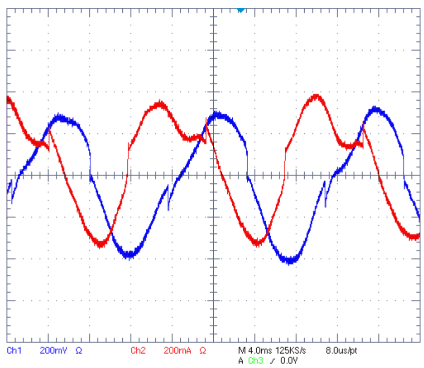

Current set-point	800mA
Micro-stepping resolution	8
Shaft speed	320rpm
Direction	CCW
Load	None

(a)

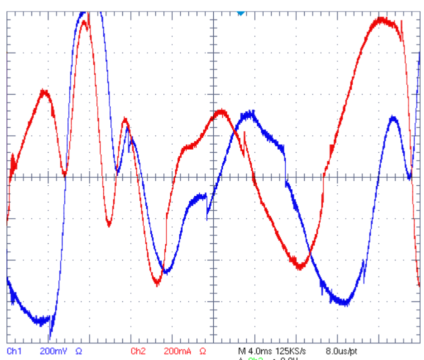

Current set-point	800mA
Micro-stepping resolution	8
Shaft speed	320rpm
Direction	CCW
Load	Fixed

(b)

Figure 38 Phase current waveforms for 8 micro-step resolution. Blue is phase-A and red is phase-B. (a) 320rpm rotation under no load and (b) 320 rpm rotation under fixed load.

5.3 *CNC Operation*

Step motors are widely used in *computer numerical control* (CNC) applications. Proposed step motor driver is also aimed to be suitable for a CNC application and the driver is tested with a CNC machine.

The CNC machine used in the tests is a desktop CNC machine with a type number of *HC501*. Besides its drilling head mechanism, it is composed of several components. There are three step motors from *Sanyo Denki Inc.* with per phase specifications of 5V - 1.4A and a holding torque of 50 oz-inch for the X, Y and Z axes. Each motor is driven by a separate step motor driver with the code name *M2MD504*. There is a power converter module for all of the electronic equipment on the machine and also a controller unit which provides the control signals for each of the three step motor drivers. The controller provides the control signals by converting the input signals generated by utilizing a CAD program *Matkap-pro v4.3* on a PC, and carried to the controller via parallel port. The connections are shown in Figure 34.

To test the step motor driver, a sample 2 dimensional model is selected where Y axis is commanded to follow a line and come back to the original position. Step motor driver unit under test is connected to the Y axis controller output and an indicator is put to the shaft of the test motor to observe if the step motor comes to its first rest position after operation of the program. Length of the path is calibrated to a value under no load and low speed to a value where the step motor under test performs a single revolution or its integral multiples.

CNC operation tests start with validating correct operation of the controller interface of the designed step motor driver by using the controller unit of the CNC machine. It is a necessity for the implemented driver to advance a single micro-step for each step pulse sent from the controller and to respond immediately after a change in direction input occurs. These requirements are confirmed by giving the same amount of step commands in the positive direction from a known rotor position and afterwards in the opposite direction. The controller-driver interface will be validated when it is observed that the rotor returns back to the initial position. An indicator,which is put on the rotating shaft as seen in Figure 35, is used to observe if the rotor returns to the initial position. The motor is rotated for multiples of one full revolution and observed whether a cumulative position error occurs or not. The test is done in a low speed light load condition to avoid any error that may occur if the system falls in the region under the pull out torque characteristic curve.

Table 7 Results for positional accuracy tests with a CNC controller.

Micro-step Resolution	*Current Set-point*	*Number of micro-step commands required for one full revolution*	*Passed/Failed*
128	1.6A(p-p)	6400	Passed
64	1.6A(p-p)	3200	Passed
32	1.6A(p-p)	1600	Passed
16	1.6A(p-p)	800	Passed
8	1.6A(p-p)	400	Passed

The accuracy of different micro-stepping resolutions is tested with the test setup described. The results are summarized in Table 7. Number of step commands needed for one full revolution are calculated with (31) where p_s is the number of full steps per revolution and μ_s is the number of micro-steps per one natural step.

$$N = \mu_s * p_s \tag{31}$$

Number of micro-steps per full step, μ_s, is calculated as one fourth of the micro-step resolution. Because, spanning all distinct micro-steps for a complete sinusoidal wave iterates over four natural steps as shown in Figure 19. Thus, for a micro-step resolution of 128, μ_s is 32. In this test, $p_s = 200$ as the test motor is a 1.8°/rev step motor.

This test is conducted with different motors and micro-stepping with different resolutions is achieved with a 1.8°/rev *mini-angle* step motor from *Astrosyn Inc*. having a type number of *23LM-C058-05H*. The second motor used is another 1.8°/rev step motor from *Sanyo Denki Inc.* having a type number of *103G770-3441*. Micro-stepping is also achieved with this motor. However, tests with a 5°/rev step motor having a type number of *57SH-46N2C*, which is the step motor used from *DPM Inc.*, was not able to return to the initial position after the micro-step commands required for one full revolution was sent from the controller, i.e., the test motor has failed to achieve micro-stepping in the desired resolutions this time. This result indicates that motor selection is an important issue to ensure proper micro-stepping operation. There are some common concerns that may limit accurate positioning in a micro-stepping realization. If the motor is optimized for full-stepping, micro-stepping operation accuracy is reduced as in this case [37].

The next step is to constitute the load-speed diagrams of the driver system. A DC motor load with a type number of *MAXON 2332.968-201* is connected to the shaft of the test motor using a flexible band to ensure a smooth start for the step motor. Load motor is operated in generator mode. A variable resistor is connected across the windings of the motor to provide an adjustable load. The step motor driver is operated for different micro-stepping resolutions. The load capacity is observed by changing speed and load torque conditions. Load torque is approximately calculated by using the formula in (32).

$$T_{load} = \frac{V_{oc} \cdot I_{load}}{w_{rotor}} \tag{32}$$

In (32), V_{oc} is the open circuit average voltage seen across the winding terminals of the load motor corresponding to the angular velocity of test motor rotor shaft or w_{rotor}. I_{load} is the value of the current that flows through the adjustable load. Immeasurable loads such as friction effects, additional inertia of the shaft or power loss on the motors are neglected in this calculation.

The test motor is operated under various speed and load conditions, where potentiometer is adjusted to six different resistance settings and the motor speed is increased until the test motor starts to lose step. The test is repeated for two different micro-step resolutions. These measurements for micro-step resolution 32 and 8 are given in Table 8 and Table 9.

Table 8 Test results for the maximum load torques achieved before the test motor starts to lose steps for micro-step resolution γ=32.

I_{load} (mA)	V_{oc} (V)	t (s/rev)	f (rev/s)	w_{rotor} (rad/s)	T_{load} (mN·m)
44	3.00	0.962	1.039	6.531	20.211
50	3.00	1.008	0.992	6.234	24.061
60	3.00	1.054	0.949	5.963	30.185
80	2.80	1.191	0.840	5.275	42.464
110	2.30	1.374	0.728	4.572	55.340
120	2.10	1.532	0.652	4.100	61.464

Table 9 Test results for the maximum load torques achieved before the test motor starts to lose steps for micro-step resolution γ=8.

I_{load} *(mA)*	V_{oc} *(V)*	*t* *(s/rev)*	*f* *(rev/s)*	w_{rotor} *(rad/s)*	T_{load} *(mN·m)*
38	2.80	1.198	0.835	5.244	20.290
43	2.80	1.198	0.835	5.244	22.960
54	2.60	1.273	0.785	4.935	28.447
69	2.40	1.348	0.742	4.661	35.527
99	2.10	1.572	0.636	3.995	52.035
100	1.90	2.210	0.452	2.843	66.830

The maximum load torque values which do not lead to any displacement error in the rotor shaft for 1/8th micro-stepping condition (γ=8) and 1/32nd micro-stepping condition (γ=32), that are shown in Table 8 and Table 9 are displayed together in Figure 39. The results have their own limitations as the current set point is below the rated value of the motor. However, the Figure 39 underlines the fact that the performance of the driver is clearly improved by increasing the micro-step resolution where all other conditions remain same as it is expected. The torque output of the motor is expected to be more stable. These results are important in this sense.

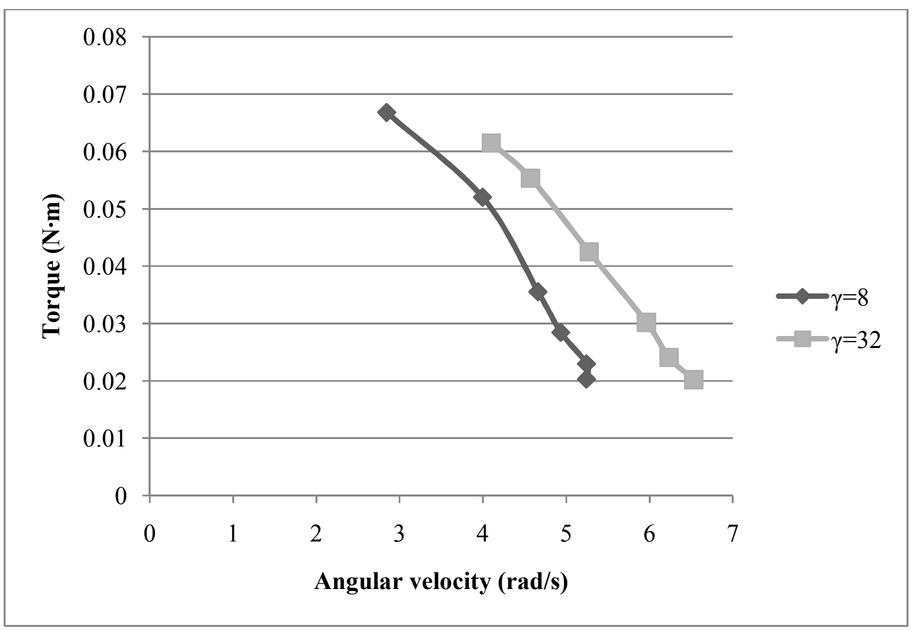

Figure 39 Load – speed curves for two different micro-stepping resolutions.

CHAPTER 6

CONCLUSIONS

This chapter begins with a summary of the work presented in this thesis. Second section provides remarks on the experimental results obtained. The third and the final section provide a discussion of possible improvements to the methods presented.

6.1 Summary

Step motors provide fine control of rotation angle and speed through discrete excitation signals. Micro-stepping enables higher precision through fractional excitation of step motor windings.

Microcontrollers enable efficient and simple generation of discrete digital signals. Low cost and effective electronic utilities are realized with the use of microcontrollers and accompanying circuitry in conjunction.

There are different driver topologies for step motor control, each having advantages and disadvantages for certain needs. Micro-stepping can be enabled using the H-bridge topology.

This thesis puts forward a step motor driver system that performs bipolar drive of 2-phase hybrid step motors. PIC18F4431, which is an 8-bit microcontroller in motor control family of Microchip Inc., forms the core of the realization of the driver presented in this thesis work. The microcontroller manages the controller – driver interface, executes the operations required for realization of micro-stepping and also provides PWM outputs of the power converter section of the driver properly. The power converter section is constructed by utilizing the full-bridge topology with discrete circuit elements. Constructed full bridge circuits provide a flexible environment to improve output power capability and enable driver algorithm selection in contrast to IC alternatives.

6.2 Discussions

A step motor driver with micro-stepping capability is designed and realized on a *PCB* in this thesis. The micro-stepping property is tested and functional operation is validated through tests. The driver is realized and tested for V_{bus} = 34Vdc and 1.6A (p-p) currents per phase. The driver works successfully by using the fixed current control method introduced in *Chapter 3*.

For an improved torque capability, two current feedback loop alternatives are constructed and the loop components are validated through functional tests. However, there are some problems encountered related to current measurements from sensing resistors which are discussed in detail in section *4.2.3*. To summarize, voltage and current waveforms on the sensing resistors are in a pulsed form. This brings a challenge to the evaluation process of the sensing current. Especially considering the cases where a high bus voltage is used in order to manipulate the current quickly, on-time of duty cycle becomes small. Also, rapid voltage and current changes occur due to the nature of the chopper configuration. Thus, there is a potential risk of observing unwanted signals on the sensing resistors occurring right after the start of the on-time originated from ground bounce issues. To overcome this problem, PIC18F4431 ADC captures input data each time a *special event trigger* occurs. Samples can be taken from unambiguous points on the waveform by this way. There is also a programmed delay element to adjust the exact sample points. This feature is also used to ensure that analog input is captured after the waveform settles and the effect of ground bounce is ended. However, sampling the voltage values that are the exact representations of the phase currents is impossible because the effects of these ripples are dominating. Since further solutions to this problem require design and implementation of a new PCB from scratch, this issue is left as a future work.

Tests reveal that increased current set-point and increased micro-stepping resolution results in higher torque output and more stable operation. Higher torque output leads to clean waveforms for phase current and thus less audible noise and less chance of missing steps. Current sensing feedback will enable efficient operation for a wider range of load and speed configurations.

6.3 *Future Work*

Step motors can operate with a fairly well performance without a position control feedback mechanism. In case of some unexpected operating conditions, a position feedback control mechanism can be helpful to detect a fault condition. Thus, adding a position sensor and a closed-loop position feedback system is expected to provide an improvement to the step motor driver.

The user interface of the step motor driver can be improved. For example, a software tool can be added to the system that allows user to simply choose the system parameters and operation modes of the driver by means of a GUI as in some industrial examples of step motor drivers.

It is also possible to enhance the driver design by adding some protection functions such as *output short circuit protection* or *over temperature protection*.

REFERENCES

[1] A. G. Thomas and F. J. Fleischauer, "The power stepping motor- a new digital actuator," *Control engineering 4*, pp. 74-81, January 1957.

[2] T. Roland Frederiksen, "Applications of the closed-loop stepping motor," *IEEE Transactions on Automatic Control*, vol. 13, no. 5, pp. 464-474, October 1968.

[3] E. K. Pritchard, "Ministepping step motor drives," in *Proc. 5th Annual Sympmosium of Incremental Motion Control Systems Devices*, 1976.

[4] Kenjo Takashi, *Stepping motors and their microprocessor controls*. Kanagawa, Japan: Clarendon Press, 1984.

[5] Muhammed F. Rahman and Aun-Neow Poo, "An application oriented test procedure for designing microstepping step motor controllers," *IEEE Transactions on Industrial Electronics*, vol. 35, no. 4, pp. 542-546, November 1988.

[6] T.C. Chin, D.P. Mital, and M.A. Jabbar, "A stepper motor controller," in *Proceedings of the International Conference on Control*, Oxford, UK, 1988, pp. 500-505.

[7] R.H. Brown and K. Srinivas, "A damping circuit for chopper driven bifilar hybrid stepper motors," in *Proceedings of the Power Electronics Specialists Conference*, Milwaukee, WI , USA, 1989, pp. 446-451.

[8] A. Imagi, M. Tomisawa, and T. Koizumi, "State and parameter estimation for step motors under actual working conditions," in *Conference Proceedings of the 16th Annual Conference on Industrial Electronics Society*, Pacific Grove, CA, USA, 1990, pp. 114-119.

[9] A.J. Blauch, M. Bodson, and J. Chiasson, "High-speed parameter estimation of stepper motors," *IEEE Transactions on Control Systems Technology*, vol. 1, no. 4, pp. 270-279, December 1993.

[10] J. Chen, D. Gaeiro, and E Stoeckert, "Spice modeling of a stepper motor with its control, drive and load," in *Proceedings of the Industry Applications Society Annual Meeting*, Seattle, WA , USA, 1990, pp. 190-195.

[11] G. Baluta, "Microstepping mode for stepper motor control," in *International Symposium on Signals, Circuits and Systems* , Iasi, Romania, 2007.

[12] Sheng-Ming Yang, Feng-Chieh Lin, and Ming-Tsung Chen, "Micro-Stepping Control of a Two-Phase Linear Stepping Motor With Three-Phase VSI Inverter for High-Speed Applications," *IEEE transactions on industrial applications*, vol. 40, no. 5, September 2004.

[13] A. Astarloa, U. Bidarte, A. Zuloaga, and I.M. de Alegria, "Reconfigurable microstepping control of stepper motors using fpga embedded ram," in *Proceedings of the 29th Annual Conference of the IEEE of the Industrial Electronics Society*, Roanoke, VA, USA, 2003, pp. 2221-2226.

[14] W. McClelland, "The application of the electricity in warships," *Journal of the Instutition of Electrical Engineers*, vol. 65, no. 369, pp. 866 - 869, September 1927.

[15] C. L. Walker, "Improvements in and connected with electromagnetic step by step signaling and syncronous rotation," 137,150, 1919.

[16] C. B. and Thain, J. H. Chicken, "Electrical Signaling Apparatus," 1,353,025, 1920.

[17] K. M. Feiertag and J.T. Donahoo, "Dynamoelectric machine," 2589999, 1952.

[18] V. Marano and D. Arrigo, "Novel fully-integrated 65W stepper motor driver IC," in *International Symposium on Power Electronics, Electrical Drives, Automation and Motion*, 2006.

[19] Pu Ji, Xiuhe Wang, Feng Lin, Rong Zhang, and Shiyong Liu, "Application of LMD18245 in two phase hybrid stepping motor driver," in *Proceedings of the Eighth International Conference on Electrical Machines and Systems*, Nanjing, China, 2005, pp. 706-709.

[20] National Semiconductor, "LMD18245 3A, 55V DMOS Full-Bridge Motor Driver ,"

Data Sheet 2006.

[21] Allegro, "A3981, Automotive, Programmable Stepper Driver," Data Sheet 2010.

[22] Allegro, "A4980, Automotive, Programmable Stepper Driver," Data Sheet 2010.

[23] ON Semiconductor, "AMIS-30523 CAN micro-stepping motor driver," Data Sheet.

[24] Peter Cox and Guido Remmerie, "Driver ICs elevate design of stepper-motor control," *Power Electronics Technology*, August 2007.

[25] Mongkol Konghirun and Chawakorn Yodsanti, "Microstepping Bipolar Drive of Two-Phase Hybrid Stepping Motor on TMS320F2808 DSC," King Mongkut's University of Technology, Thonburi, Application Report 2008.

[26] A. Bellini, C. Concari, G. Franceschini, and A. Toscani, "Mixed-mode pwm for high-performance stepping motors," *IEEE Transactions on Industrial Electronics*, vol. 54, no. 6, pp. 3167-3177, December 2007.

[27] Ngoc Quy Le and Jae Wook Jeon, "An open-loop stepper motor driver based on fpga," in *Proccedings of the International Conference on Control, Automation and Systems*, Seoul, Korea, 2007, pp. 1322-1326.

[28] Xiaodong Zhang, Junjun He, and Chunlei Sheng, "An approach of micro-stepping control for the step motors based on fpga," in *Proceedings of the IEEE International Conference on Industrial Technology*, Hong Kong, PRC, 2005, pp. 125-130.

[29] Sorin Manea, "Stepper Motor Control with dsPIC® DSCs," Microchip Technology Inc., Application Note 2009.

[30] Ran Zhang, Xiuhe Wang, Yubo Yang, and Dongwei Qiao, "Design of two-phase hybrid stepping motor driver with current closed-loop control based on PIC18F2331," in *Proceedings of the International Conference on Electrical Machines and Systems*, Wuhan, PRC, 2009, pp. 2998-3001.

[31] Microchip Technology Inc, "PIC18F2331/2431/4331/4431 Data Sheet," 2003.

[32] International Rectifier, "IR2110 High and low side driver," Data Sheet 2005.

[33] T.S. Weerakoon and L. Samaranayake, "Development of a Novel Drive Topology for a Five Phase Stepper Motor," in *IEEE Region 10 Colloquium and the Third ICIIS*, 2008.

[34] Alexandru Morar, "Stepper motor model for dynamic simulation," *Achta Electronica*, vol. 44, no. 2, pp. 117-122, 2003.

[35] M. Zribi and J. Chiasson, "Position Control of a PM Stepper Motor by Exact Linearization," *IEEE transactions on automatic control*, vol. 36, no. 5, pp. 620-625, May 1991.

[36] David J. Griffiths, "Maxwell's stress tensor," in *Introduction to Electrodynamics*.: Benjamin Cummings Inc., 2008, pp. 351 - 352.

[37] Ericsson. Industrial Circuits Application Note: Stepper Motor Basics. [Online]. http://www.solarbotics.net/library.html

[38] G. Baluta and M. Coteata, "Precision microstepping system for bipolar stepper motor control," in *Conference Proceedings of the International Aegean Conference on Electrical Machines and Power Electronics*, Muğla, Turkey, 2007, pp. 291-296.

[39] Acarnley, *Stepping Motors: a guide to modern theory and practice*, 3rd ed. England: Peter Peregrinus Ltd, 1992.

[40] Douglas W. Jones, "Current limiting for stepping motors," in *Handbook of small electric motors*, Alan W. Yeadon William H. Yeadon, Ed.: McGraw-Hill, 2001, ch. 10.

[41] ST Microeelectronics, "Microstepping Stepper Motor Drive Using Peak Detecting Current Control," Application Note 2004.

[42] K. L. Sh and Hui Li, "Optimized PWM strategy based on genetic algorithms," *IEEE Transactions on industrial electronics*, vol. 52, no. 5, pp. 1458-1561, October 2005.

[43] L. Peng, Y. Kang, X. Pei, and J. Chen, "A novel pwm technique in digital control," *IEEE Transactions on Industrial Electronics*, vol. 54, no. 1, pp. 338-346, February

2007.

[44] Carl Blake and Chris Bull, "IGBT or MOSFET: Choose Wisely," International Rectifier, Application Note 2006.

[45] Maxim Integrated Products, "Power supply engineer's guide to calculate dissipation for MOSFETs in high-power supplies ," Application Note 2002.

[46] (2005) H-bridge secrets. [Online]. http://www.modularcircuits.com/h-bridge_secrets1.htm

[47] International Rectifier, "IRF640N," Data Sheet 2004.

[48] ON Semiconductor, "MUR420 Switchmode power rectifiers," Data Sheet 2010.

[49] Ansoft, Ansoft-Simplorer V7.0. A power electronics simulation software, 2004.

[50] Ned Mohan, Tore M. Undeland, and William P. Robbins, *Power Electronics Converters, Applications, and Design*, 3rd ed.: John Wiley and Sons, Inc., 2003.

[51] International Rectifier, "HV floating MOS-gate driver ICs," Application Note 2007.

[52] A. Merello, A. Rugginenti, and M. Grasso, "Using monolithic high voltage gate drivers," International Rectifier, Design tips.

[53] Fairchild Semiconductor, "UF4001-UF4007 Fast Rectifiers," Data Sheet 2005.